An analytical model for solute transport through a water-saturated single fracture and permeable rock matrix

J. E. Houseworth,[1] D. Asahina,[1] and J. T. Birkholzer[1]

The problem of solute transport through a water-saturated single fracture in a permeable rock matrix is examined using an analytical modeling approach. A closed-form analytical solution is obtained that accounts for transverse and longitudinal advective transport in the fracture and matrix and transverse diffusion in the matrix. The solution also accounts for both diffusive and advective solute exchange between the fracture and matrix and a general solute source position in either the fracture or matrix. The novel features are the incorporation of advective transport in the matrix and a general source position into a closed-form solution for the solute-transport problem. Examples of the solution behavior are presented, which demonstrate the effects of matrix advection in combination with advection along the fracture, transverse diffusion in the matrix for solute release in the fracture and matrix. A semianalytical solution in the form of a superposition integral is also derived that includes these transport features, plus independent levels of longitudinal diffusion and dispersion in the matrix and fracture, respectively. Examples are presented that include advective transport in the fracture and matrix, longitudinal and transverse diffusion in the matrix, longitudinal dispersion in the fracture, as well as solute release from the fracture and matrix. An approximate criterion is proposed to evaluate the significance of longitudinal diffusion and dispersion relative to longitudinal spreading caused by fracture-matrix interaction.

1 Introduction

Solute transport in groundwater flow through frac- tured rock is a subject that has been investigated for nuclear waste disposal and other environmental groundwater contamination problems [National Research Council, 1996]. Fractures are a common feature of consolidated rock systems and typically present much higher permeability than unfractured rock matrix, such that flow through fractures often dominates overall flow behavior. Matrix, on the other hand, typically dominates the overall pore volume of a fractured rock. These attributes often lead to much higher solute-transport velocities through fractures than in unfractured rock or unconsolidated soils [Berkowitz, 2002]. This behavior often makes fracture flow and transport critical characteristics to examine for any geologic site where solute transport is a concern. However, despite their importance, fractures remain a difficult feature to represent accurately in mathematical models for groundwater flow and transport [Matthäi et al., 2009; Wu and Pruess, 2000]. Flow through fractures displays highly heterogeneous and complex flow patterns controlled by small-scale fracture features. Furthermore, transport processes at small scales that govern fracture-matrix exchange can dramatically influence larger-scale transport behavior [Grisak and Pickens, 1980].

Transport through saturated fractured rock was first investigated in an analytical model by Neretnieks [1980]. Tang et al. [1981] extended this work to include the effects of longitudinal dispersion in the fracture, and Sudicky and Frind [1982] and Maloszewski and Zuber [1985] further generalized the transport problem from a single fracture to a system of parallel fractures with interceding rock matrix. Sharifi Haddad et al. [2012] developed a semianalytical model of solute transport in a system of parallel fractures for a radially symmetric flow field associated with well injection. Maloszewski and Zuber [1990] considered the effects of linear kinetic interactions between solute and the rock for a single fracture and rock matrix. All of these models were restricted to advective transport in the fracture, transverse diffusion in the matrix, and diffusive fracture-matrix solute exchange. A review of these modeling approaches among others is provided by Bodin et al. [2003a, 2003b]. Cihan and Tyner [2011] developed exact analytical solutions for advective transport through cylindrical macropores and diffusive exchange with a soil matrix, for an instantaneous release of solute into a macropore, a constant concentration of solute at the top of a macropore, and a pulse release of solute into a macropore.

[1]Earth Sciences Division, Lawrence Berkeley National Laboratory, Berkeley, California, USA.

Corresponding author: J. E. Houseworth, Earth Sciences Division, Lawrence Berkeley National Laboratory, Berkeley, CA 94720, USA. (jehouseworth@lbl.gov)

They also compared their analytical solutions with numerical simulations that included longitudinal and transverse matrix advection and longitudinal dispersion in the macropore. *Roubinet et al*. [2012] added the effects of transverse dispersion in a fracture and longitudinal diffusion in the matrix to these mechanisms, and found that transverse dispersion in fractures had little effect on solute transport, but that longitudinal diffusion in the matrix becomes important at low Peclet numbers. The solution provided by *Roubinet et al*. [2012] also is capable of treating spatially varying and time-dependent source conditions.

[4] Other modeling efforts have focused on advective-dominated systems. *Birkhölzer et al*. [1993a, 1993b] present an analytical model for transport through a two-dimensional fracture network and permeable rock matrix under conditions in which fracture-matrix exchange is dominated by advective processes, such that diffusion could be neglected. A diffusion-advection number was also developed to help ascertain conditions for which diffusive fracture-matrix exchange is negligible compared with advective fracture-matrix exchange. The methodology developed by *Birkhölzer et al*. [1993a, 1993b] was used by *Rubin et al*. [1996] to investigate a tracer slug injection in a fractured rock with permeable rock matrix, and by *Rubin et al*. [1997] to investigate transport for cases with slow advective velocities in the fracture. *Odling and Roden* [1997] used a numerical model to study transport in fracture networks embedded in a permeable rock matrix, focusing on the role the permeable rock matrix plays when fracture networks have limited connectivity, including fractures that are disconnected from the network.

[5] *Cortis and Birkholzer* [2008] and *Geiger et al*. [2010] have utilized a continuous-time random-walk numerical method to investigate the effects of diffusion and advection in fractured, permeable rock. Transport calculations for a two-dimensional fracture network having a range of fracture and matrix permeabilities were used to identify the parameter ranges over which matrix advection has a significant role or may be neglected.

[6] *Houseworth* [2006] extended analytical modeling approaches for unsaturated flow, and included longitudinal and transverse flow and advective transport in the matrix, as well as advective and diffusive transport between the fracture and rock matrix. Longitudinal diffusion/dispersion was not included for the fracture or matrix, because this greatly simplifies the analytical model and is a reasonable approximation in some cases. For an unsaturated fractured rock, local differences in capillary conditions between the fracture and the rock matrix tend to dominate fracture-matrix flow exchange, such that flow exchange is more likely to result either in fracture discharge into the matrix or convergent matrix flow into the fracture.

[7] An analogous problem was analyzed by *Zhan et al*. [2009] for transport through a saturated system consisting of an aquifer confined above and below by aquitards of infinite extent. The analogy is that the aquifer corresponds to the fracture and the aquitards correspond to the rock matrix surrounding a fracture. Longitudinal advection and longitudinal and transverse dispersion were included as transport mechanisms in the aquifer. Transport in the aquitards was limited to the transverse direction but included both advection and diffusion. The general solution led to analytical results in the Laplace domain that required numerical inversion. Transverse dispersion in the aquifer and a more general treatment of transverse advection were new features introduced into the analyses. *Zhan et al*. [2009] compared their solution with previously derived solutions in which solute concentration was assumed to be transversely well mixed in the aquifer. They concluded that accounting for transverse solute gradients and transverse solute-transport processes in the aquifer had a significant impact on the results. In addition, the total solute mass entering the aquitard from the aquifer was found to be sensitive to the Peclet number for advective and diffusive transport in the aquitards.

[8] The analytical model presented here is for solute transport during steady state saturated flow occurring in a single fracture and a porous, permeable rock matrix. This model goes beyond existing analytical models by including the combination of lateral matrix diffusion and flow through the matrix in any direction relative to the orientation of the fracture axis, as well as flow through the fracture. Thus, the flow direction in the matrix and fracture may have components both parallel to and orthogonal to the fracture axis, leading to fracture-matrix exchange through cross-flow [*Birkhölzer and Rouve*, 1994]. Diffusive fracture-matrix exchange and general diffusive transport orthogonal to the fracture axis in the rock matrix is also included. The location of solute release as an instantaneous point source is generalized for an arbitrary point within the model domain. Closed-form analytical solutions for transport are obtained for these conditions neglecting longitudinal diffusion and dispersion. Solutions are also developed including simultaneous dispersive transport along the fracture and longitudinal diffusion in the matrix. These solutions take the form of superposition integrals of the closed-form results.

2. Flow Model

[9] Transport processes are considered for a two-dimensional, saturated flow system with a single fracture embedded in a permeable rock matrix. Specification of the flow field is a necessary first step to define the transport problem. The permeability of the rock matrix is taken to be homogeneous and isotropic and the fracture is assigned a different, higher, permeability than the matrix along the fracture axis. It also has permeability equal to that of the matrix in the direction transverse to the fracture axis. This anisotropy in the fracture simplifies the flow problem. In general, the transverse permeability of the fracture is generally not too significant because of the narrow transverse dimension of the fracture, unless this permeability is much lower than the matrix and represents a flow barrier. Flow is also restricted to steady state conditions, implying steady state pressure boundary conditions. For simplicity, the flow process will be discussed for a situation in which flow is driven exclusively by pressure differences.

[10] The flow system investigated is a generalization of the flow driven by a simple uniform pressure gradient aligned with the fracture axis. To understand the steady state, two-dimensional flow field, the flow system is diagrammed in Figure 1 with the fracture axis oriented in the same direction as the z axis. The corners of the rectangular flow domain are the origin, $z = x = 0$; $z = L_z$, $x = 0$;

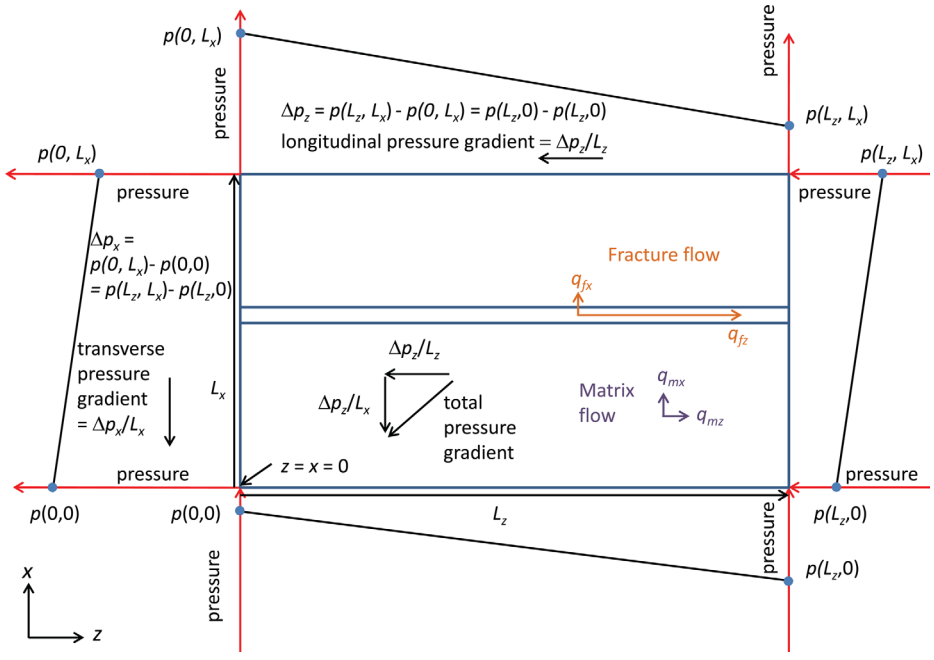

Figure 1. Steady state flow field for single fracture in permeable rock matrix.

$z = L_z$, $x = L_x$; and $z = 0$, $x = L_x$, moving around the rectangle in counterclockwise order. The red arrows at the corners of the domain are axes displaying pressure. The pressures at the corners are set so that pressure drops across the domain in the longitudinal and transverse directions are uniform. From this configuration, it is clear that there will be a uniform transverse flow within the domain with the water flux rates $q_{fx} = q_{mx}$. Longitudinal water flux rates within the matrix (q_{mz}) and the fracture (q_{fz}) are uniform within their respective domains; however, $q_{fz} > q_{mz}$. The total pressure gradient is also shown and is uniform across the entire flow domain.

[11] Rotating the flow system in Figure 1 such that the rotated z coordinate, z', aligns with the total pressure gradient results in the flow diagram given in Figure 2. This flow system is equivalent to the system shown in Figure 1. Because the z' coordinate is parallel to the total pressure gradient, there is no flow along the constant x' boundaries (upper and lower boundaries in Figure 2) and the constant z' boundaries (left and right boundaries in Figure 2) coincide with contours of constant pressure. The flow field (relative to the fracture) remains the same as in Figure 1. Through this rotation, the flow field in Figure 1 is shown to be equivalent to a flow field resulting from a uniform pressure gradient that is not (necessarily) aligned with the fracture axis.

[12] The transport problem to be solved is assumed to be sufficiently far from the pressure boundaries that any effects of these boundaries on transport are negligible. The configuration as shown in Figure 1 is used to compute transport processes, with the longitudinal direction defined to be the same direction as the axis of the fracture and the transverse direction is defined to be orthogonal to the fracture.

3. Transport Model

[13] A schematic diagram of the transport process to be analyzed is given in Figure 3. Longitudinal transport by advection occurs in both the matrix and fracture; transverse advective and diffusive transport occurs in the matrix. Solute exchange occurs through transverse advective and diffusive mechanisms. Because flow occurs in the matrix, there is formally both diffusion and hydrodynamic dispersion occurring in the matrix [*Bear*, 1972]. For the model development, we assume that matrix diffusion dominates in comparison with hydrodynamic dispersion and will be referred to as *matrix diffusion* rather than *matrix dispersion*. Further discussion of this issue is given in section 5. Transverse exchange between the fracture and matrix are treated through specifying source-sink terms at the fracture-matrix interface. Solute sorption and decay in both fracture and matrix are included. Solute release can be located at any

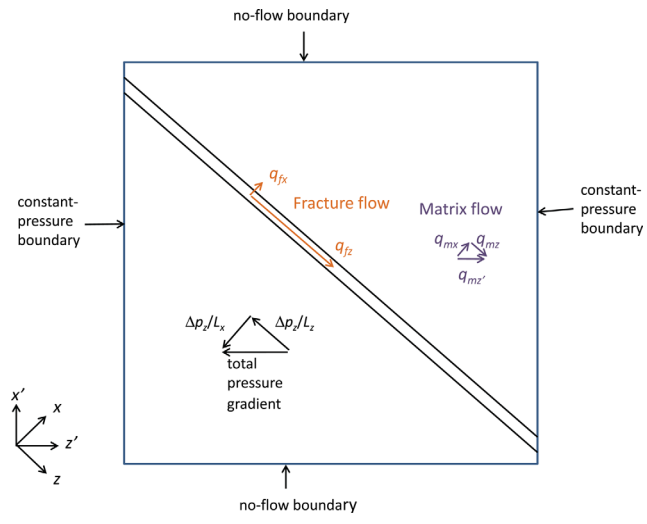

Figure 2. Rotated steady state flow field for single fracture in permeable rock matrix, equivalent to that shown in Figure 1.

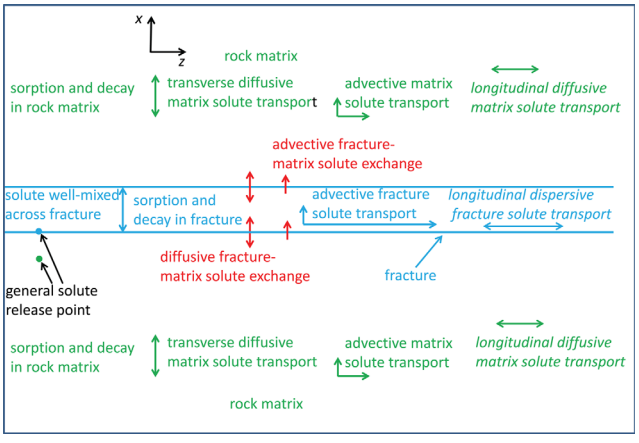

Figure 3. Solute transport mechanisms for single-fracture in permeable rock matrix. Note: fracture processes in blue, matrix processes in green, and fracture-matrix exchange processes in red. Longitudinal dispersion/diffusion processes are in italic font to recognize the development of solutions in this paper both neglecting and including these processes.

point within the matrix or in the fracture. Because of a general solute release location and uni-directional transverse flow, solute concentrations are not, in general, symmetric about the fracture, and mathematical solutions for solute concentration on each side of the fracture must be developed.

[14] Also shown in Figure 3 is the assumption of a well-mixed solute within the fracture in the transverse direction; therefore, there is no need to define a transverse fracture velocity or transverse diffusion in the fracture for lateral transport within the fracture. As a result, the fracture transport problem is one-dimensional in the longitudinal direction.

[15] Certain restrictions are required for the well mixed assumption to be valid. Consider the time for a solute released at a point within the fracture aperture or the aquifer to become well mixed across the fracture aperture through diffusion or dispersion. Classical diffusion theory shows that the diffusive mixing time t_d is proportional to b^2/D_T, where b is the fracture aperture and D_T is the transverse diffusion (or dispersion) coefficient. Investigations into transport during flow through channels indicate that the mixing time required for solute concentrations to become uniform across the cross section is given by, $t_d = b^2/4D_T$ [*Dentz and Carrera*, 2007]. This time should be much smaller than other times of interest, such as the fracture advective time scale, $t_f = z_e/v_f$, where z_e is the downstream solute travel distance of interest and v_f is the advective velocity in the fracture, giving the restriction $v_f b^2/D_T z_e \ll 4$. For a system that includes both diffusion and transverse advection, the mixing time may be compared with the advective travel time across a fracture, $t_m = b/v_{ft}$, where v_{ft} is the advective velocity in the fracture transverse to the fracture axis, leading to a restriction on the transverse Peclet number, $v_{ft} b/D_T \ll 4$.

[16] The validity of the well mixed assumption imposes more restrictive conditions for larger fracture apertures. Natural fracture apertures generally range from a few microns up to a few millimeters [e.g., *Nelson*, 1985; *Pyrak-Nolte and Morris*, 2000; *Hooker et al.*, 2013]. Solute transverse dispersion coefficients inside fractures are not well known. For open fractures, solute diffusion in water may be appropriate, generally on the order of 10^{-9} m^2/s. Fractures with filling material would have reduced levels of molecular diffusion as a result of tortuosity effects, but would also experience additional mixing caused by transverse hydrodynamic dispersion associated with flow through the filled fracture. Using a value of 10^{-9} m^2/s for transverse dispersion, the diffusive mixing time for a large fracture with a 1 cm aperture is 2.5×10^4 s, or about 7 h. A fracture with a 1 mm aperture would have a diffusive mixing time of 250 s and for an aperture of 0.1 mm, the diffusive mixing time is 2.5 s. As a rough approximation, assume that "<<4" in the criteria above may be interpreted to mean "<0.4." Then, over a 100 m travel distance, this leads to restrictions on the longitudinal fracture velocity to be less than about 35, 3.5×10^3, and 3.5×10^5 m/d, respectively, for the three cases (apertures of 1 cm, 1 mm, and 0.1 mm). Similarly, the transverse velocity in the fracture for these cases would be restricted to values less than about 3.5×10^{-3}, 3.5×10^{-2}, and 0.35 m/d, respectively, to be consistent with the well mixed assumption. These restrictions are expected to be easily met in many circumstances.

[17] Solutions will first be obtained neglecting longitudinal diffusion/dispersion in the fracture and rock matrix, indicated in Figure 3 by the italic font for these processes. Neglecting longitudinal diffusion/dispersion simplifies the analysis and allows for a closed-form solution of the transport problem; in many cases, this is a suitable approximation. A method to include these transport mechanisms is subsequently derived, and analytical results including these processes are presented.

[18] The model to be analyzed does not address certain phenomena that have been identified and remain research questions concerning transport in fractured rock systems. Processes not analyzed here include scale-dependent diffusion effects, exchange between flowing and stagnant water within fractures, channeled flow in fractures due to asperities, and fracture skin effects [*Liu et al.*, 2004, *Zhou et al.*, 2007, *Robinson et al.*, 1998].

3.1. Conservation Equation for Solute Transport in the Fracture

[19] For a single fracture in a porous rock matrix, the tracer mass conservation equation for the fracture is:

$$\phi_f\left(\frac{\partial c_f}{\partial t}+\lambda c_f\right)+\rho_{bf}\left(\frac{\partial c_{fa}}{\partial t}+\lambda c_{fa}\right)+q_f\frac{\partial c_f}{\partial z} = A_{vfm}\left(\frac{1}{2}\phi_m D_m\frac{\partial c_m}{\partial x}\Big|_{x=0^s}+\frac{1}{2}\phi_m D_m\frac{\partial c_m}{\partial x}\Big|_{x=0^o} + \frac{1}{2}q_{fm}|_{x=0^s}c_m|_{x=0^s}+\frac{1}{2}q_{fm}\Big|_{x=0^o}c_m\Big|_{x=0^o}\right) \quad (1)$$

with initial and boundary conditions as follows:

$$c_f(z,0)=0 \quad (2)$$

$$\lim_{z\to\infty} c_f(z,t)=0 \quad (3)$$

$$c_f(z,t)=c_m(z,0^s,t)=c_m(z,0^o,t) \quad (4)$$

where, c_f is aqueous solute concentration in the fracture water, c_{fa} is the mass of solute sorbed per unit mass of minerals in the fracture, c_m is the aqueous solute concentration in the matrix, and q_f is the water flux in the fracture. The independent variables t, z, and x represent time, longitudinal distance, and transverse distance, respectively. The first and second terms in equation (1) represent the rate of change in solute mass dissolved and sorbed to mineral surfaces, respectively, including radioactive decay represented by the decay constant λ. The intrinsic porosity of the fracture (i.e., the fracture pore volume divided by the fracture bulk volume) is ϕ_f, and ρ_{bf} is the bulk density of minerals in the fracture. If the fracture has no minerals within the fracture itself, c_{fa} would be defined as the sorbed solute per unit area of mineral surface represented by the fracture walls, in which case ρ_{bf} becomes the mineral surface area per unit fracture bulk volume. In some cases, it may be necessary to incorporate sorption on both fracture walls and minerals. The third term in equation (1) represents the net longitudinal advective flux of solute at a point for a longitudinal fracture water flux rate q_f. Longitudinal diffusive/dispersive transport in the fracture is not included.

[20] Terms on the right-hand side of equation (1) represent advective and diffusive solute exchange between the fracture and matrix. The matrix diffusion coefficient is D_m, ϕ_m is the matrix porosity, and $A_{vfm} = 2/b$ is the fracture-matrix interface area per unit fracture bulk volume where b is the fracture aperture. The x axis is defined separately for each side of the fracture. The origin for each x axis is zero at the fracture wall, and then increases moving away from the fracture. Fracture-matrix interface conditions are distinguished with respect to the side of the fracture where the tracer is released. The side of the fracture where tracer is released is designated with a superscript or subscript s denoting the source side of the fracture, and with a superscript or subscript o for the opposite side of the fracture from where the tracer is released. The fracture-matrix water fluxes are denoted by $q_{fm}|_{x=0^s}$ and $q_{fm}|_{x=0^o}$. Both are positive for flow away from the fracture (the positive x direction for each side). Given the steady state flow fields described earlier,

$$q_{fm}|_{x=0^s} = -q_{fm}|_{x=0^o} \tag{5}$$

[21] The conservation equation requires a constitutive model to link sorbed and solute concentrations. The simplest form of such a relationship, used here, is the linear, infinite capacity sorption model,

$$c_{fa} = K_{df} c_f \tag{6}$$

and an analogous relationship for sorption in the matrix,

$$c_{ma} = K_{dm} c_m \tag{7}$$

where K_{df} and K_{dm} are the fracture and matrix sorption coefficients, respectively, and c_{ma} is the sorbed solute mass per unit mass rock matrix. Using this sorption model and conditions in equations (4) and (5), equation (1) may be rewritten more compactly using dimensionless retardation factors, $R_f = 1 + \rho_{bf} K_{df}/\phi_f$ and $R_m = 1 + \rho_{bm} K_{dm}/\phi_m$ for the fracture and matrix, respectively,

$$\frac{\partial c_f}{\partial t} + \lambda c_f + v_f \frac{\partial c_f}{\partial z} = A_{vfm} \frac{\phi_m R_m}{\phi_f R_f} \frac{D_m^*}{2} \left(\frac{\partial c_m}{\partial x}\bigg|_{x=0^s} + \frac{\partial c_m}{\partial x}\bigg|_{x=0^o} \right) \tag{8}$$

where ρ_{bm} is the bulk mineral density in the matrix, $v_f = q_f/\phi_f R_f$ is the fracture advective transport velocity, and $D_m^* = D_m/R_m$ is the retarded diffusion coefficient. Further simplification is achieved using the following transformations to decay-neutral concentrations:

$$c_{f\lambda} = c_f \exp(\lambda t) \tag{9}$$

$$c_{m\lambda} = c_m \exp(\lambda t) \tag{10}$$

giving

$$\frac{\partial c_{f\lambda}}{\partial t} + v_f \frac{\partial c_{f\lambda}}{\partial z} = A_{vfm} \frac{\phi_m R_m}{\phi_f R_f} \frac{D_m^*}{2} \left(\frac{\partial c_{m\lambda}}{\partial x}\bigg|_{x=0^s} + \frac{\partial c_{m\lambda}}{\partial x}\bigg|_{x=0^o} \right) \tag{11}$$

with initial and boundary conditions

$$c_{f\lambda}(z, 0) = 0 \tag{12}$$

$$\lim_{z\to\infty} c_{f\lambda}(z, t) = 0 \tag{13}$$

$$c_{f\lambda}(z, t) = c_{m\lambda}(z, 0^s, t) = c_{m\lambda}(z, 0^o, t) \tag{14}$$

3.2. Conservation Equation for Solute Transport in the Matrix

[22] The conservation equation for solute mass in the matrix is:

$$\begin{aligned} &\phi_m \left(\frac{\partial c_{mk}}{\partial t} + \lambda c_{mk} \right) + \rho_{bm} \left(\frac{\partial c_{mak}}{\partial t} + \lambda c_{mak} \right) \\ &+ q_{mz} \frac{\partial c_{mk}}{\partial z} + q_{mxk} \frac{\partial c_{mk}}{\partial x} = \phi_m D_m \frac{\partial^2 c_{mk}}{\partial x^2} \end{aligned} \tag{15}$$

where subscript k refers to the source (s) or the opposite (o) side of the fracture with respect to the tracer release location. The transverse flux, q_{mxk}, is defined to be positive when flowing away from the fracture for each side; therefore, $q_{mxs} = -q_{mxo}$. The solute concentration in matrix pore water is c_{mk} and the solute sorbed per unit mass of matrix minerals is c_{mak}; ρ_{bm} is the bulk density of minerals in the matrix. As for the fracture conservation equation, the first two terms represent the rate of change in dissolved and sorbed solute mass, respectively, and the third term is the net longitudinal advective flux of solute at a point for a longitudinal matrix-water flux rate q_{mz}. The fourth term is the net transverse advective flux of solute at a point for a transverse matrix-water flux rate q_{mx}. The term on the right-hand side of equation (15) is the net transverse diffusive flux of solute. As for the fracture conservation equation, diffusive/dispersive transport in the longitudinal direction is not included.

[23] The initial and boundary conditions for the matrix conservation equation are:

$$c_{ms}(z,x,0) = \frac{bM_0}{A_f \phi_m R_m}\delta(x-x_0)\delta(z) \tag{16}$$

$$c_{mo}(z,x,0) = 0 \tag{17}$$

$$c_{mk}(z,0,t) = c_f(z,t) \tag{18}$$

[24] Equation (16) gives the initial condition on the source side of the fracture, while (17) gives the initial condition on the opposite side of the fracture from the source release point. Note that if $x_0 = 0$, the initial condition represents tracer release in the fracture because of the boundary condition (18). The mass of tracer released is M_0, A_f is the fracture cross-sectional area orthogonal to the fracture axis, and δ is the Dirac delta function that is dimensionally an inverse length. The effective third dimension for defining the initial solute-mass concentration is given by A_f/b. Equation (15) may be simplified using previously defined quantities to be

$$\frac{\partial c_{mk\lambda}}{\partial t} + v_{mz}\frac{\partial c_{mk\lambda}}{\partial z} + v_{mxk}\frac{\partial c_{mk\lambda}}{\partial x} = D_m^* \frac{\partial^2 c_{mk\lambda}}{\partial x^2} \tag{19}$$

where $v_{mxk} = q_{mxk}/(\phi_m R_m)$ and $v_{mz} = q_{mz}/(\phi_m R_m)$ and the initial and boundary conditions become

$$c_{m\lambda s}(z,x,0) = \frac{bM_0}{A_f \phi_m R_m}\delta(x-x_0)\delta(z) \tag{20}$$

$$c_{m\lambda o}(z,x,0) = 0 \tag{21}$$

$$c_{m\lambda k}(z,0,t) = c_f(z,t) \tag{22}$$

$$\lim_{x\to\infty} c_{m\lambda k}(z,x,t) = 0 \tag{23}$$

3.3. Transformation to a Moving Reference Frame

[25] Solution of the coupled fracture-matrix conservation equations requires a reduction in dimensionality of the matrix conservation equation, with explicit dependence on gradients in both longitudinal and transverse directions. This can be accomplished by introducing a coordinate transformation to a reference frame moving in the z direction at a velocity of v_{mz}. Let

$$\varsigma = z - v_{mz}t \tag{24}$$

[26] Then the fracture conservation equation becomes

$$\frac{\partial c_{f\lambda}}{\partial t} + v_f^* \frac{\partial c_{f\lambda}}{\partial \varsigma} = A_{vfm}\frac{\phi_m R_m}{\phi_f R_f}\frac{D_m^*}{2}\left(\left.\frac{\partial c_{m\lambda}}{\partial x}\right|_{x=0^s} + \left.\frac{\partial c_{m\lambda}}{\partial x}\right|_{x=0^o}\right) \tag{25}$$

with initial and boundary conditions

$$c_{f\lambda}(\varsigma,0) = 0 \tag{26}$$

$$\lim_{\varsigma\to\infty} c_{f\lambda}(\varsigma,t) = 0 \tag{27}$$

where $v_f^* = v_f - v_{mz}$. The matrix conservation equation becomes

$$\frac{\partial c_{mk\lambda}}{\partial t} + v_{mxk}\frac{\partial c_{mk\lambda}}{\partial x} = D_m^* \frac{\partial^2 c_{mk\lambda}}{\partial x^2} \tag{28}$$

with boundary and initial conditions

$$c_{m\lambda s}(\varsigma,x,0) = \frac{bM_0}{A_f \phi_m R_m}\delta(x-x_0)\delta(\varsigma) \tag{29}$$

$$c_{m\lambda o}(\varsigma,x,0) = 0 \tag{30}$$

$$c_{m\lambda k}(\varsigma,0,t) = c_f(\varsigma,t) \tag{31}$$

$$\lim_{x\to\infty} c_{m\lambda k}(\varsigma,x,t) = 0 \tag{32}$$

3.4. Dimensionless Form

[27] The conservation equations for the fracture (25)–(27) are put into the following dimensionless form:

$$\frac{\partial c_{fd}}{\partial \tau} + \frac{\partial c_{fd}}{\partial \xi} = \frac{1}{2}\left(\left.\frac{1}{Pe}\frac{\partial c_{md}}{\partial \eta}\right|_{\eta=0^s} + \left.\frac{1}{Pe}\frac{\partial c_{md}}{\partial \eta}\right|_{\eta=0^o}\right) \tag{33}$$

$$c_{fd}(\xi,0) = 0 \tag{34}$$

$$\lim_{\xi\to\infty} c_{fd}(\xi,\tau) = 0 \tag{35}$$

and equations (28)–(32) become:

$$\frac{\partial c_{mdk}}{\partial \tau} + V_k\frac{\partial c_{mdk}}{\partial \eta} = \frac{1}{Pe}\frac{\partial^2 c_{mdk}}{\partial \eta^2} \tag{36}$$

$$c_{mds}(\xi,\eta,0) = \delta(\xi)\delta(\eta-\eta_0) \tag{37}$$

$$c_{mdo}(\xi,\eta,0) = 0 \tag{38}$$

$$c_{mdk}(\xi,0,\tau) = c_{fd}(\xi,\tau) \tag{39}$$

$$\lim_{\eta\to\infty} c_{mdk}(\xi,\eta,\tau) = 0 \tag{40}$$

where the independent variables are $\tau = v_f^* t/\ell$, $\xi = \varsigma/\ell = (z - v_{mz}t)/\ell$, $\eta = x/\ell$ using the length scale $\ell = \left(b\phi_f R_f\right)/(2\phi_m R_m)$, dimensionless concentrations $c_{fd} = \left(A_f \phi_f R_f \ell c_{f\lambda}\right)/(2M_0)$ and $c_{md} = \left(A_f \phi_f R_f \ell c_{m\lambda}\right)/(2M_0)$, and parameters $Pe = v_f^* \ell / D_m^*$ and $V_k = v_{mxk}/v_f^*$. The dimensionless delta functions at $t = 0$ are given by $\delta(\eta - \eta_0) = \ell\delta(x - x_0)$ and $\delta(\xi) = \ell\delta(z)$.

3.5. Solution of the Conservation Equations

[28] A Laplace-transform method is used to solve these equations, similar to the solution method presented in *Houseworth* [2006]. A solution of the Laplace-transformed matrix concentration is first found in terms of the independent variables and fracture concentration. This result is used to solve for the Laplace-transformed fracture concentration. Then Laplace inversions are performed to determine the concentrations in the physical time domain.

[29] The Lapace-transformed concentrations are defined by

$$H(\tau)c_{fd}(\xi,\tau) = \frac{1}{2\pi i}\int_{c-i\infty}^{c+i\infty} \hat{c}_{fd}(\xi,s)e^{s\tau}ds \tag{41}$$

$$H(\tau)c_{mdk}(\xi,\eta,\tau) = \frac{1}{2\pi i}\int_{c-i\infty}^{c+i\infty} \hat{c}_{mdk}(\xi,\eta,s)e^{s\tau}ds \tag{42}$$

where $H(\tau)$ is the step function defined by $H(\tau)=1$ for $\tau \geq 0$ and 0 otherwise.

[30] Substituting for $c_{mds}(\xi,\eta,\tau)$ into the equation (36) for the source side of the fracture gives

$$\frac{\partial^2 \hat{c}_{mds}}{\partial \eta^2} - PeV_s\frac{\partial \hat{c}_{mds}}{\partial \eta} - sPe\hat{c}_{mds} = -Pe\delta(\xi)\delta(\eta-\eta_0) \tag{43}$$

[31] This equation is solved subject to the boundary conditions

$$\hat{c}_{mds}(\xi,0,\tau) = \hat{c}_{fd}(\xi,\tau) \tag{44}$$

$$\lim_{\eta\to\infty} \hat{c}_{mds}(\xi,\eta,s) = 0 \tag{45}$$

[32] Equation (43) is solved by dividing the domain into two parts, where $\hat{c}^+_{mds}$ is used for $\eta > \eta_0$ and $\hat{c}^-_{mds}$ for $\eta < \eta_0$. This division of the domain results in the following continuity requirements between $\hat{c}^+_{mds}$ and $\hat{c}^-_{mds}$:

$$\lim \eta_0^+ \to \eta_0, \eta_0^- \to \eta_0 \quad \hat{c}^+_{mds}(\xi,\eta_0^+,s) = \hat{c}^-_{mds}(\xi,\eta_0^-,s) \tag{46}$$

and

$$\lim \eta_0^+ \to \eta_0, \eta_0^- \to \eta_0 \quad \frac{\partial \hat{c}^+_{mds}}{\partial \eta}(\xi,\eta_0^+,s) - \frac{\partial \hat{c}^-_{mds}}{\partial \eta}(\xi,\eta_0^-,s) = -Pe\delta(\xi) \tag{47}$$

where η_0^- to η_0^+ are approaching η_0 from smaller and larger values of η, respectively. The second consistency requirement (47) arises from integrating equation (43) over η from η_0^- to η_0^+, using (44) and the requirement that the integral of $\hat{c}_{mds}$ is zero in the limit as η_0^- to η_0^+ approaches η_0. Within each domain, equation (43) is a homogeneous, second-order ordinary differential equation in η with constant coefficients. The solution within each domain introduces two unknown coefficients that are determined using the two boundary conditions and two consistency requirements. The solutions are:

$$\begin{aligned}\hat{c}^-_{mds}(\xi,\eta,s) = &\left\{\hat{c}_{fd}(\xi,s) - \frac{Pe\delta(\xi)}{2\sqrt{\frac{Pe^2V^2}{4}+sPe}}\exp\left[-\left\{\frac{PeV_s}{2}+\sqrt{\frac{Pe^2V^2}{4}+sPe}\right\}\eta_0\right]\right\}\exp\left[\left\{\frac{PeV_s}{2}-\sqrt{\frac{Pe^2V^2}{4}+sPe}\right\}\eta\right]\\ &+\frac{Pe\delta(\xi)}{2\sqrt{\frac{Pe^2V^2}{4}+sPe}}\exp\left[-\left\{\frac{PeV_s}{2}+\sqrt{\frac{Pe^2V^2}{4}+sPe}\right\}\eta_0\right]\exp\left[\left\{\frac{PeV_s}{2}+\sqrt{\frac{Pe^2V^2}{4}+sPe}\right\}\eta\right]\end{aligned} \tag{48}$$

$$\begin{aligned}\hat{c}^+_{mds}(\xi,\eta,s) = &\left\{\hat{c}_{fd}(\xi,s) + \frac{Pe\delta(\xi)}{\sqrt{\frac{Pe^2V^2}{4}+sPe}}\exp\left[-\frac{PeV_s}{2}\eta_0\right]\sinh\left(\sqrt{\frac{Pe^2V^2}{4}+sPe}\eta_0\right)\right\}\\ &\times\exp\left[\left\{\frac{PeV_s}{2}-\sqrt{\frac{Pe^2V^2}{4}+sPe}\right\}\eta\right]\end{aligned} \tag{49}$$

[33] For the flow field investigated here, $V_s = -V_o$. Therefore, $V_s^2 = V_o^2$, and is denoted as V^2.

[34] For the side opposite the matrix source, the Laplace-transformed conservation equation is

$$\frac{\partial^2 \hat{c}_{mdo}}{\partial \eta^2} - PeV_o\frac{\partial \hat{c}_{mdo}}{\partial \eta} - sPe\hat{c}_{mdo} \tag{50}$$

subject to boundary conditions

$$\hat{c}_{mdo}(\xi,0,s) = \hat{c}_{fd}(\xi,s) \tag{51}$$

$$\lim_{\eta\to\infty} \hat{c}_{md0}(\xi,\eta,s) = 0 \tag{52}$$

[35] The solution is

$$\hat{c}_{mdo}(\xi,\eta,s) = \hat{c}_{fd}(\xi,s)\exp\left[\left\{\frac{PeV_o}{2}-\sqrt{\frac{Pe^2V^2}{4}+sPe}\right\}\eta\right] \tag{53}$$

[36] Finally, the fracture conservation equation under a Laplace transform is

$$\frac{\partial \hat{c}_{fd}}{\partial \xi} + s\hat{c}_{fd} - \frac{1}{2Pe}\frac{\partial \hat{c}^-_{mds}}{\partial \eta}\bigg|_{\eta=0^s} - \frac{1}{2Pe}\frac{\partial \hat{c}_{mdo}}{\partial \eta}\bigg|_{\eta=0^o} = 0 \tag{54}$$

[37] Substituting for $\hat{c}^-_{mds}$ and $\hat{c}_{mdo}$ from equations (48) and (53), respectively, gives

$$\frac{\partial \hat{c}_{fd}}{\partial \xi} + s\hat{c}_{fd} - \frac{\hat{c}_{fd}}{2Pe}\left\{\frac{PeV_s}{2} - \sqrt{\frac{Pe^2V^2}{4} + sPe}\right\} - \frac{\hat{c}_{fd}}{2Pe}\left\{\frac{PeV_o}{2} - \sqrt{\frac{Pe^2V^2}{4} + sPe}\right\} = \frac{\delta(\xi)}{2}\exp\left[-\left\{\frac{PeV_s}{2} + \sqrt{\frac{Pe^2V^2}{4} + sPe}\right\}\eta_0\right] \tag{55}$$

which has the solution

$$\hat{c}_{fd} = \frac{1}{2}\exp\left\{-\frac{PeV_s}{2}\eta_0\right\}\exp\{-s\xi\}\exp\left\{-\sqrt{\frac{V^2}{4} + \frac{s}{Pe}}(\xi + Pe\eta_0)\right\}H(\xi) \tag{56}$$

[38] Substituting the result (56) into (41) and evaluating the Laplace inversion yields

$$c_{fd}(\xi,\tau) = H(\tau-\xi)H(\xi)\frac{\xi + Pe\eta_0}{4\sqrt{\pi}\sqrt{Pe}(\tau-\xi)^{\frac{3}{2}}}\exp\left(-\frac{PeV_s}{2}\eta_0\right) \times\exp\left(-\frac{(\xi+Pe\eta_0)^2}{4Pe(\tau-\xi)} - \frac{PeV^2(\tau-\xi)}{4}\right) \tag{57}$$

[39] Similar inversions are performed to determine the matrix concentration for the side of the fracture opposite the source, which is found to be

$$c_{mdo}(\xi,\eta,\tau) = H(\tau-\xi)H(\xi)\exp\left(\frac{PeV_o(\eta+\eta_0)}{2}\right)\frac{\xi + Pe(\eta+\eta_0)}{4\sqrt{\pi}\sqrt{Pe}(\tau-\xi)^{\frac{3}{2}}} \times\exp\left\{-\frac{(\xi+Pe(\eta+\eta_0))^2}{4Pe(\tau-\xi)} - \frac{PeV^2(\tau-\xi)}{4}\right\} \tag{58}$$

and for the matrix on the source side of the fracture,

$$c_{mds}(\xi,\eta,\tau) = H(\tau-\xi)H(\xi)\exp\left\{\frac{PeV_s(\eta-\eta_0)}{2}\right\}\frac{\xi + Pe(\eta+\eta_0)}{4\sqrt{\pi}\sqrt{Pe}(\tau-\xi)^{\frac{3}{2}}} \times\exp\left(-\frac{(\xi+Pe(\eta+\eta_0))^2}{4Pe(\tau-\xi)} - \frac{PeV^2(\tau-\xi)}{4}\right) + \frac{\sqrt{Pe}\delta(\xi)}{2\sqrt{\pi\tau}}\exp\left\{\frac{PeV_s}{2}(\eta-\eta_0) - \frac{PeV^2\tau}{4}\right\} \times\left[\exp\left\{-\frac{Pe(\eta-\eta_0)^2}{4\tau}\right\} - \exp\left\{-\frac{Pe(\eta+\eta_0)^2}{4\tau}\right\}\right] \tag{59}$$

[40] Furthermore, recognizing that $c_{fd}(\xi,\tau) = c_{mds}(\xi,0,\tau) = c_{mdo}(\xi,0,\tau)$, the solution for concentration is completely specified by (58) and (59). The matrix solute concentration on the source side of the fracture, equation (59), has a term involving $\delta(\xi)$. This term represents solute in the matrix that has not interacted with the fracture and moves at the matrix advection velocity as a concentration spike at $\xi = 0$. This infinite concentration occurs because the model does not include longitudinal solute diffusion in the matrix. The closed-form solutions in (57)–(59) have been verified directly by substitution into equations (33)–(40).

[41] For some applications, it is useful to have the solution in the form of cumulative-mass arrival at a downstream location as a function of time. Such a mass arrival curve from an instantaneous point source may be computed from integrals of the solutions presented in this section, with the resulting formulae given in the section A1. The cumulative mass results have been compared with previously published solutions (see section A2) for cases without matrix advection.

4. Solution Behavior Without Longitudinal Diffusion/Dispersion

[42] The solution behavior is examined for a set of six cases in which the flow velocities and source positions are varied, using a fracture within a domain that is 100 m long as measured along the fracture axis. The domain orthogonal to the fracture is unbounded. Hydrogeologic properties consistent with the flow velocities used are given in Table 1. The intrinsic fracture permeability corresponds roughly to a parallel-plate permeability for a fracture with an aperture of 10^{-4} m. For a fracture spacing of 1 m, the bulk fracture permeability would be 1.18×10^{-13} m^2.

[43] Table 2 provides the range of values for transport parameters and Table 3 presents the fixed parameters for the cases investigated. Note that sorption (K_{df} and K_{dm}) coefficients, the decay constant (λ), and all longitudinal diffusion/dispersion coefficients are zero for the examples in this section. In these examples, the pressure gradient direction is varied with respect to the fracture axis. Table 2 shows this angle ranges from 0° to 84.4°. As the angle between the pressure gradient and fracture axis vary, both fracture and matrix velocities are affected by the changing components of the pressure gradient. For Cases 1–3, the source release occurs in the fracture and for Cases 4–6 the source release occurs in the matrix 0.5 m offset from the fracture. As mentioned before, all source releases are assumed to be instantaneous at time $t = 0$. These examples involve long time frames, up to 10^5 years, as a result of the selected matrix permeability, domain length, magnitude

Table 1. Hydrogeologic Parameters and Domain Investigated

Matrix Permeability (m^2)	Intrinsic Fracture Permeability (m^2)	Regional Gradient of Hydraulic Head	Doman Length (m)
3.06×10^{-16}	1.18×10^{-9}	0.01	100

Table 2. Flow and Transport Parameters Varied

	Primary						Dimensionless			
Case	v_f (m/s)	v_{mz} (m/s)	v_{mxs} (m/s)	Angle (°)	x_0 (m)	t (days)	Pe	V_s	η_0	τ
1	1.16×10^{-4}	3×10^{-10}	0	0	0	200	580	0	0	4.01×10^{6}
2	8.2×10^{-5}	2.12×10^{-10}	-2.12×10^{-10}	45	0	200	410	-2.59×10^{-5}	0	2.83×10^{6}
3	1.14×10^{-5}	2.94×10^{-11}	-2.99×10^{-10}	84.4	0	200	56.9	-2.63×10^{-5}	0	3.93×10^{5}
4	1.16×10^{-4}	3×10^{-10}	0	0	−0.5	2000	580	0	10^{3}	4.01×10^{7}
5	8.2×10^{-5}	2.12×10^{-10}	-2.12×10^{-10}	45	−0.5	2000	410	-2.59×10^{-5}	10^{3}	2.83×10^{7}
6	1.14×10^{-5}	2.94×10^{-11}	-2.99×10^{-10}	84.4	−0.5	2000	56.9	-2.63×10^{-5}	10^{3}	3.93×10^{6}

and direction of the hydraulic gradient, and matrix porosity given in Tables 1–3. While such time frames may not be of interest for some applications, we present results to the display entire arrival curves from an instantaneous point source for completeness. Time frames of this magnitude are not unusual for problems involving nuclear waste disposal, and safety assessments of disposal systems typically encompass $10^5 - 10^6$ years [*Birkholzer et al.*, 2012].

[44] An example of the analytical model transport responses using equations (58) and (59) is given in Figure 4 for solute release in the fracture and flow parallel to the fracture. Figure 4a shows the contour pattern for concentration at 200 days after source release, with the elongated profile indicative of the enhanced longitudinal transport along the fracture. The symmetrical transverse spreading is a result of transverse diffusion from the fracture into the matrix. Advective longitudinal transport in the matrix cannot be resolved in this figure, because the trailing concentration front is at a longitudinal position of only 0.005 m. The cumulative-mass arrival and mass-arrival rates at 100 m from the origin are given in Figures 4b and 4c, respectively. Cumulative-mass-arrival curves are computed using equations (A3), (A6), and (A7) from Appendix A, and the mass-arrival rates are computed from the time derivatives of these equations. Mass arrivals and arrival rates are given for the fracture and for each side of the matrix. The "matrix source" and "matrix opposite" terms in Figures 4b and 4c refer to cumulative mass and mass-arrival rates in the matrix on the negative and positive sides of the fracture, respectively, in terms of the transverse coordinate. For this case, the matrix-mass arrivals and arrival rates are the same on both sides of the fracture, because of the symmetry of this problem about the fracture axis. The trailing edge of the mass-arrival rate in Figure 4c shows a sharp decrease near 10,000 years. This is close to the time required for a solute to arrive 100 m downstream moving at the matrix advection velocity (10,563 years). Because there is no longitudinal diffusion or dispersion, any solute that has had minimal interaction with the fracture will arrive at the 100 m boundary close to this time.

[45] An example with an oblique cross-flow is shown in Figure 5. The only difference between this case and Case 1 in Figure 4 is that the hydraulic gradient is at a 45° angle to the fracture axis. The asymmetry of the contour plot relative to the fracture in Figure 5a is a result of the matrix cross-flow component orthogonal to the fracture. As a result of cross-flow, the highest concentration portion of the profile is displaced laterally, which impedes longitudinal transport of the main solute mass as shown in Figures 5b and 5c as compared with Figures 4b and 4c Solute interaction with the fracture is also reduced, limiting dispersion through fracture-matrix interaction, and resulting in higher peak concentrations. A more substantial mass of solute arrives in the matrix at the downstream boundary as shown in Figure 5b, arriving through the matrix on the downstream side (positive x coordinate side) of the fracture relative to matrix cross-flow.

[46] An example with stronger cross-flow is shown in Figure 6, in which the hydraulic gradient is at an 84.4° angle to the fracture axis. Contours are shown in Figure 6a at 200 days and in Figure 6b at 6000 days. The relatively slower velocity in the fracture and greater advective losses of solute to the matrix reduce the rate of solute advance as compared with Figures 4 and 5. Peak solute concentrations are correspondingly higher than in Figures 4 and 5. By comparison with Figure 4, where diffusion is the only mechanism for fracture-matrix exchange, this example clearly shows that matrix cross-flow can have a significant influence on fracture-matrix exchange. The effects of cross-flow create significant lateral movement of solute relative to the fracture, limiting the interaction of solute with the fracture. Such effects would be moderated in a fracture-network setting as a result of interactions with other fractures in the network. This is also seen clearly in the mass-arrival and arrival-rate curves in Figures 6c and 6d. A large fraction of solute travels to the downstream location mainly through the matrix, as indicated in Figure 6c by the large increase in cumulative-mass arrivals close to the matrix travel time, 100 m divided by the matrix longitudinal velocity, or 1.08×10^5 years.

Table 3. Parameters Used for All Cases

Primary										Dimensionless
ϕ_f	ϕ_m	K_{df} (m^3/kg)	K_{dm} (m^3/kg)	b (m)	ℓ (m)	D_m (m^2/s) (transverse)	A_f (m^2)	M_0 (kg)	λ (s^{-1})	V_ℓ
1	0.1	0	0	10^{-4}	5×10^{-4}	10^{-10}	1	1	0	2.59×10^{-6}

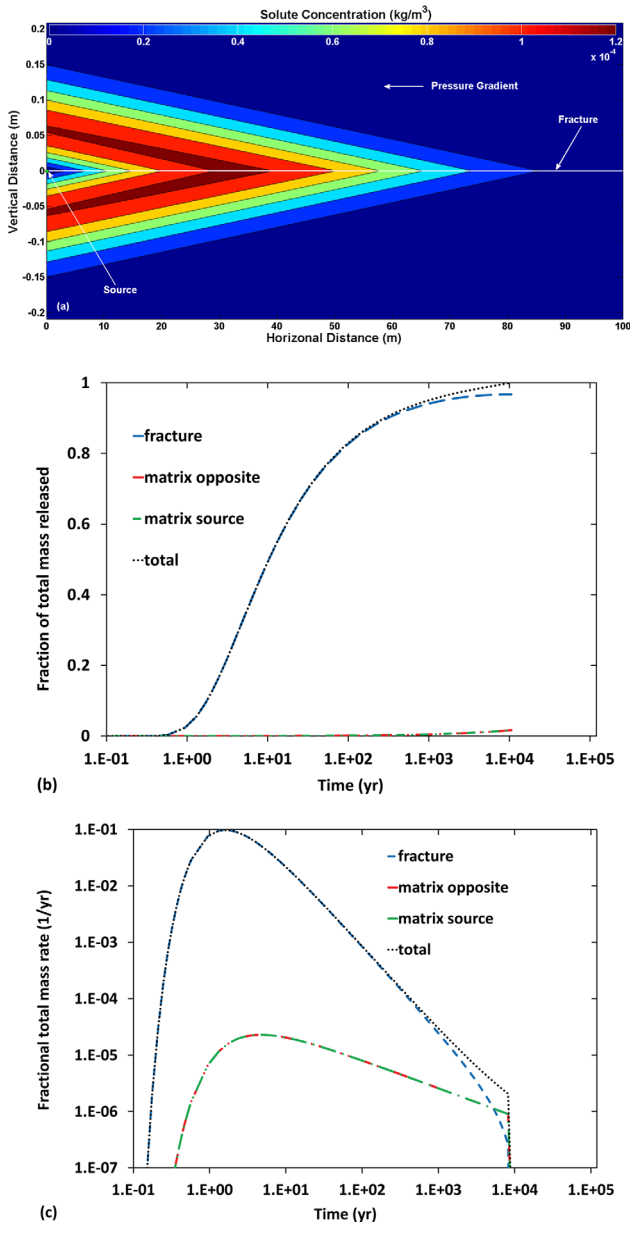

Figure 4. Case 1: Transport results for matrix flow parallel to the fracture and solute release in the fracture. (a) Concentration contours at 200 days; (b) cumulative-mass arrivals at 100 m; (c) mass-arrival rates at 100 m.

[47] The profile in Figure 7 is a result of modifying case 1 (Figure 4, pressure gradient parallel to the fracture) by moving the source into the matrix by 0.5 m. Solute transport through the fracture is delayed because of the source location, and the contours in Figure 7a are at 2000 days instead of 200 days as in Figure 4a. The resulting profile shows the reduced degree of interaction between the solute and the fracture caused by the source offset position. Concentrations in the figure are limited to solute mass that has diffused from the source to interact with the fracture and thereby disperse longitudinally. The trailing concentration spike in the matrix represents solute that has not interacted with the fracture and has an infinite concentration, as a result of no longitudinal diffusion in the matrix. The early parts of the cumulative mass-arrival and mass-arrival-rate curves in Figures 7b and 7c are delayed relative to those in Figures 4b and 4c and the peak mass-arrival rate is significantly higher for Case 1.

[48] Figure 8 shows a case that is comparable with Case 2 (Figure 5, pressure gradient at a 45°angle to the fracture), except that the source is located in the matrix 0.5 m from the fracture. The trailing concentration spike is present in the matrix as a result of solute in the matrix that has not yet interacted with the fracture. Concentration contours in Figure 8a are slightly displaced to the side of the fracture opposite the source as compared with Figure 7a, because of the transverse flow in the matrix in that direction. Note that for Figure 8a, the simulation time is 2000 days compared with 200 days for Figure 5a. The reduced fracture velocity

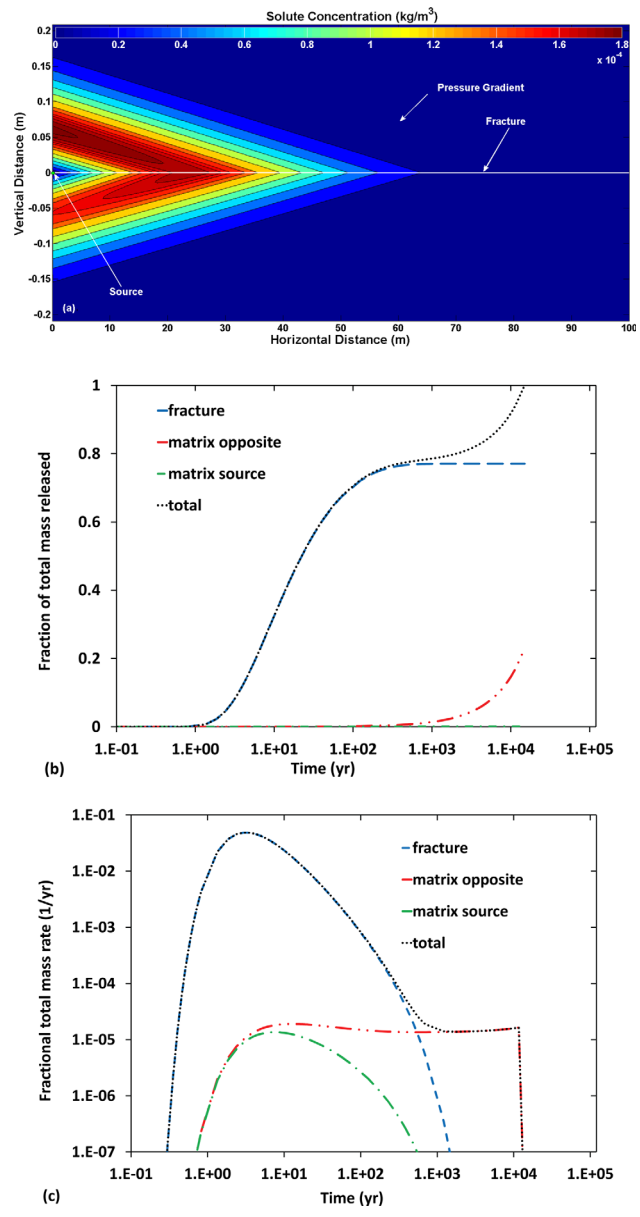

Figure 5. Case 2: Same as Case 1 but with the hydraulic gradient at a 45°angle to the fracture. (a) Concentration contours at 200 days; (b) cumulative-mass arrivals at 100 m; (c) mass-arrival rates at 100 m.

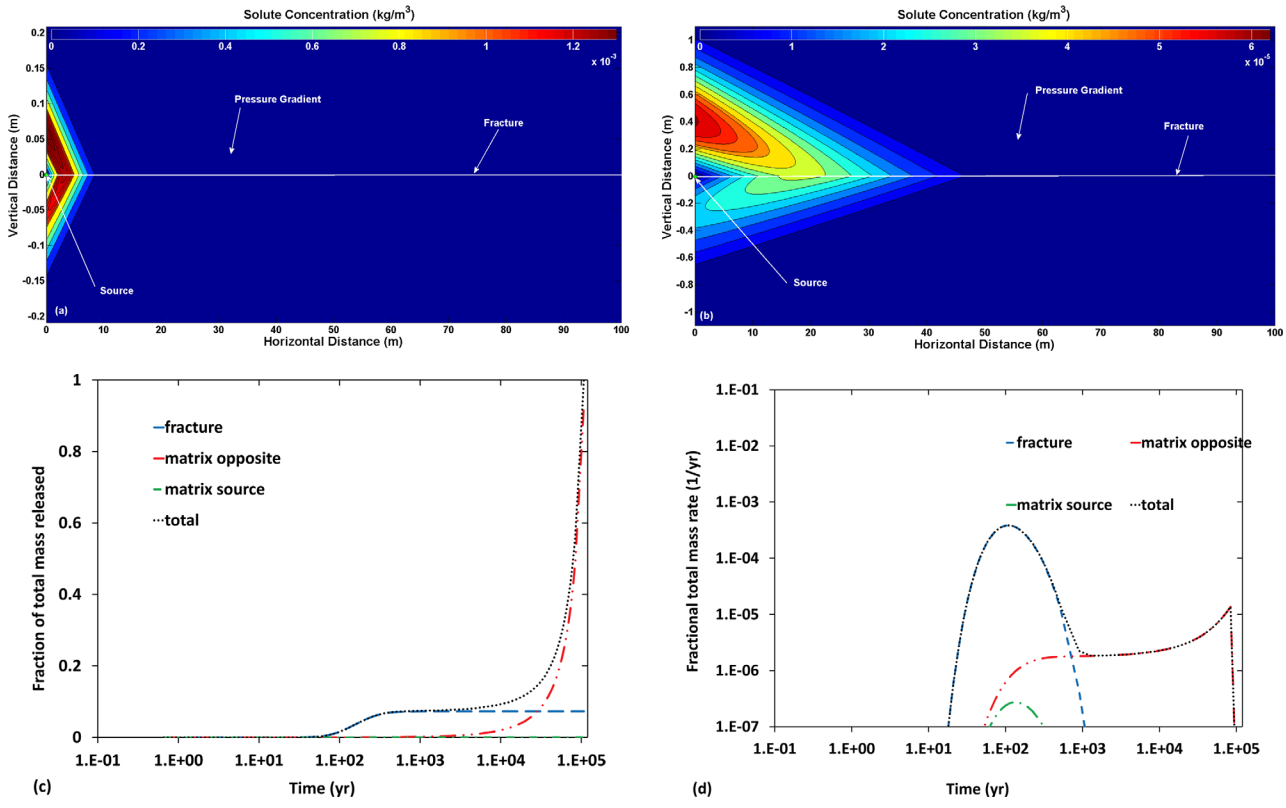

Figure 6. Case 3: Same as Case 1 but with the hydraulic gradient at a 84.4° angle to the fracture. (a) Concentration contours at 200 days; (b) concentration at 6000 days—note expanded y axis scale; (c) cumulative-mass arrivals at 100 m; (d) mass-arrival rates at 100 m. Note that the transverse scale is expanded for this high cross-flow velocity case.

and increased matrix cross-flow cause the latter part of the cumulative arrival curve and mass-arrival rates in Figures 8b and 8c to be delayed in comparison with Case 2.

[49] Figure 9 shows Case 6, comparable with Case 3 (Figure 6, pressure gradient at a 84.4°angle to the fracture), except that the source is located in the matrix 0.5 m from the fracture. Contours are shown in Figure 9a at 2000 days and in Figure 9b at 40,000 days. The relatively slower velocity in the fracture reduces the rate of advance of the solute as compared with Figures 7 and 8. The concentration contours in Figure 9b are significantly displaced to the side of the fracture opposite the source, because of the transverse flow within the matrix in that direction. The reduced fracture velocity and increased matrix cross-flow cause the latter part of the cumulative-arrival and arrival-rate curves in Figures 9c and 9d to be delayed, similar to Case 3. If the cross-flow direction is reversed for Cases 5 and 6, even more solute travels entirely (or almost entirely) within the matrix to the downstream observation point.

5. Longitudinal Diffusion and Dispersion

[50] Analytical models of advective-dispersive transport in a fracture with diffusive exchange with a porous matrix have been given by *Tang et al.* [1981], *Sudicky and Frind* [1982], and *Maloszewski and Zuber* [1985, 1990]. However, these models did not include advective transport in the matrix or longitudinal diffusion in the matrix. For the purposes of the following analysis, diffusion in the matrix will be assumed to dominate dispersive effects, so that diffusive transport is approximately isotropic. This condition is expected when advective velocities in the matrix are sufficiently small [*Bear*, 1972]. Under certain conditions, these restrictions may be relaxed; this will be discussed following the results for the restricted case below.

[51] Consider a simple case in which fracture and matrix longitudinal and transverse velocities are the same, v_z and v_x, respectively, and isotropic diffusion with an apparent diffusion coefficient of D^*. The release of an instantaneous point source of solute, mass M_0, would result in a solute distribution, $\mathbb{C}(z,x,t)$, that can be written down immediately as the product of independent one-dimensional solutions for the x and z directions with constant drifts [*Carslaw and Jaeger*, 1959, sections 10.7 and 1.15]:

$$\mathbb{C}(z,x,t) = \frac{M_0}{4\pi D^* t}\exp\left\{-\frac{(z-v_z t)^2+(x-v_x t)^2}{4D^* t}\right\} \tag{60}$$

[52] This solution can also be obtained by starting with the solution excluding longitudinal diffusion:

$$c(z,x,t) = \frac{M_0\delta(z-v_z t)}{\sqrt{4\pi D^* t}}\exp\left\{-\frac{(x-v_x t)^2}{4D^* t}\right\} \tag{61}$$

[53] The fundamental solution for longitudinal diffusion from an instantaneous point source is

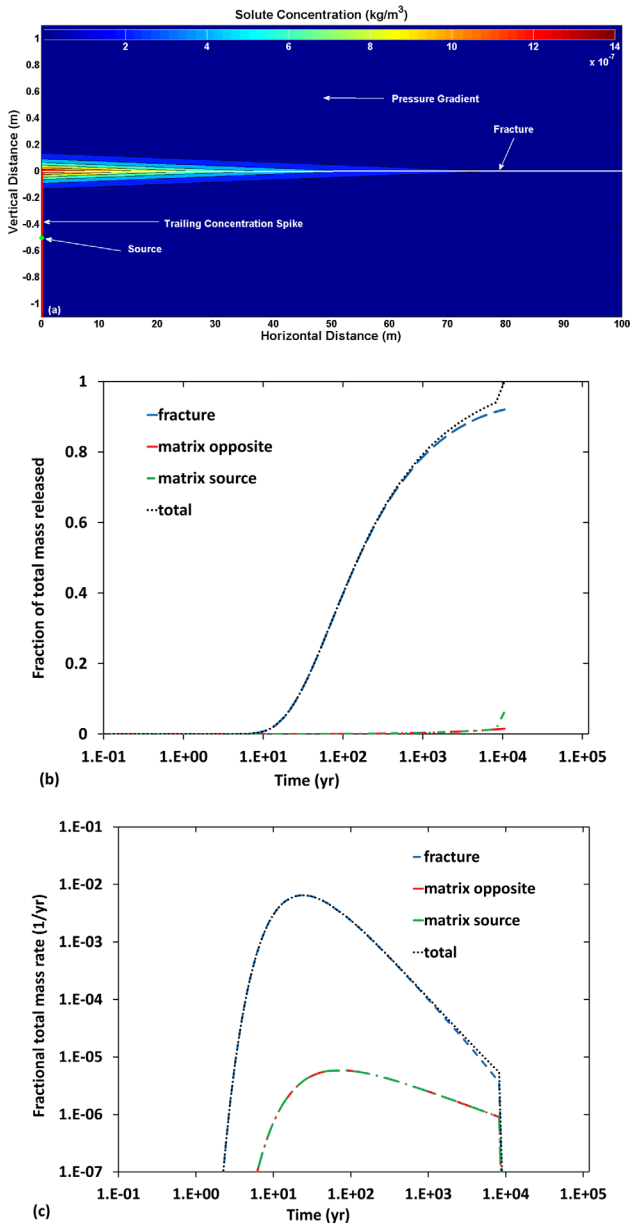

Figure 7. Case 4: Same as Case 1 but with source located in matrix 0.5 m from fracture. (a) Concentration contours at 2000 days; (b) cumulative-mass arrivals at 100 m; (c) mass-arrival rates at 100 m.

$$\tilde{c}(z,t) = \frac{M(z,x,t)}{\sqrt{4\pi D^* t}} \exp\left(-\frac{z^2}{4D^* t}\right) \tag{62}$$

[54] Equation (61) may be used as a source term (which is now spatially distributed in the x direction) for a longitudinal diffusion process given by (62). This amounts to freezing advection and lateral diffusion over the time period t to assess solute diffusion in the longitudinal direction. This can be done because diffusion in the longitudinal direction is independent of diffusion in the transverse direction, and independent of advection in both directions. The resulting concentration including longitudinal diffusion takes the form of a superposition integral, involving mass releases at all longitudinal positions according to the spatial distribution of mass at time t, $M(z,x,t)$:

$$\mathbb{C}(z,x,t) = \int_{-\infty}^{\infty} \tilde{c}(z-z',t)\,dM(z',x,t) \tag{63}$$

[55] Letting $dM(z',x,t) = c(z',x,t)dz'$ gives

$$\begin{aligned}\mathbb{C}(z,x,t) &= \int_{-\infty}^{\infty} c(z',x,t)\tilde{c}(z-z',t)dz' \\ &= \frac{M_0}{4\pi D^* t}\exp\left\{-\frac{(z-v_z t)^2 + (x-v_x t)^2}{4D^* t}\right\}\end{aligned} \tag{64}$$

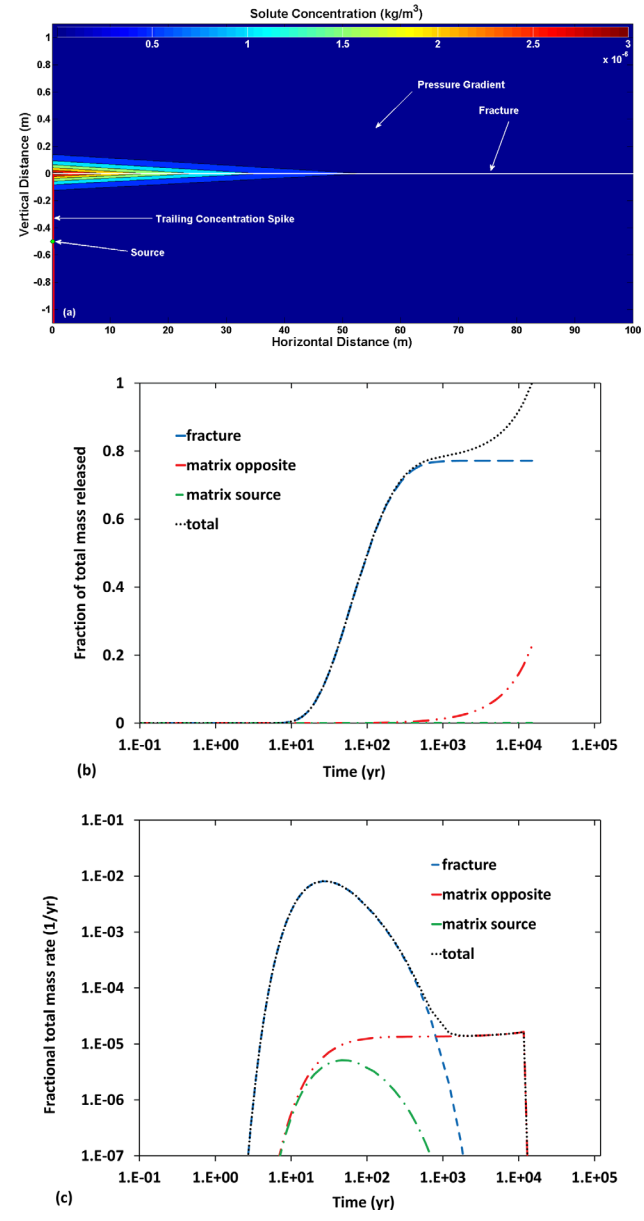

Figure 8. Case 5: Same as Case 2 but with source located in matrix 0.5 m from fracture. (a) Concentration contours at 2000 days; (b) cumulative-mass arrivals at 100 m; (c) mass-arrival rates at 100 m.

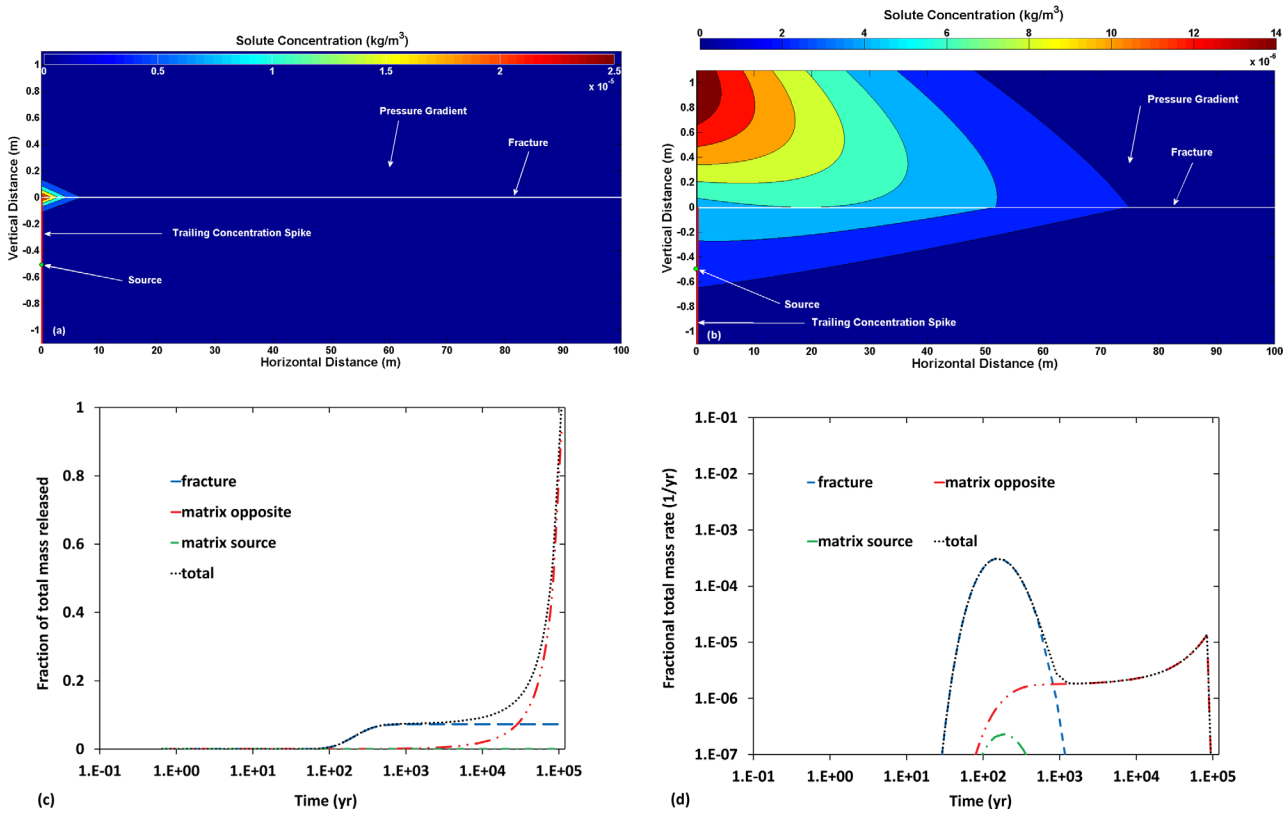

Figure 9. Case 6: Same as Case 3 but with source located in matrix 0.5 m from fracture. (a) Concentration contours at 2000 days; (b) concentration contours at 40,000 days; (c) cumulative-mass arrivals at 100 m; (d) mass-arrival rates at 100 m.

which is the same result as in equation (60). The same superposition concept was recognized by *Thacker* [1976] for incorporating longitudinal dispersion occurring within shear layers into a global transport solution for shear dispersion.

[56] This same procedure for incorporating longitudinal diffusion may be used even if the advective velocity in the z direction is a function of the transverse position x. It is perhaps simpler to visualize this method by focusing on individual solute molecular paths. For the case with no longitudinal diffusion, a solute molecule drifts in the longitudinal direction according to the local longitudinal velocity, and also drifts in the transverse direction by the constant transverse velocity. Transverse movement is also caused by a transverse random walk associated with diffusion. The addition of longitudinal diffusion results in a longitudinal random walk superimposed on the original particle movement, but does not impact the transverse movement of the solute or the distribution of longitudinal flow velocities experienced by the solute. The only effect of longitudinal diffusion is to randomize the longitudinal position of the solute according to the longitudinal diffusive process.

[57] A solution analogous to equation (61) excluding longitudinal diffusion cannot be solved for a case in which the advective velocity in the z direction is a general function of the transverse position, x. However, the result for c_{mdk} from section 3 represents this type of solution for the particular case of a single fracture and matrix involving two longitudinal velocities. Consider again the case in which longitudinal diffusion is the same in the fracture and matrix, and matrix diffusion is isotropic. Since all solute diffuses at the same rate, the solution of the transport problem including longitudinal diffusion is given by

$$\mathbb{C}_{mdk}(z,x,t) = \int_{v_{mz}t}^{v_f t} \frac{c_{mdk}\left(\frac{z'-v_{mz}t}{\ell}, \frac{x}{\ell}, \frac{v_f^* t}{\ell}\right)}{\sqrt{4\pi D_m^* t}} \exp\left\{-\frac{(z-z')^2}{4D_m^* t}\right\} dz' \quad (65)$$

[58] The limits of integration extend exclusively over the range of longitudinal positions that have nonzero values of solute concentration from the source function. Putting equation (65) into dimensionless form yields

$$\mathbb{C}_{mdk}(\xi,\eta,\tau) = \int_0^{\tau} c_{mdk}(\xi',\eta,\tau) \frac{\sqrt{Pe}}{\sqrt{4\pi\tau}} \exp\left\{-\frac{Pe(\xi-\xi')^2}{4\tau}\right\} d\xi' \quad (66)$$

[59] This method may be extended to address different rates of diffusion/dispersion in the fracture and matrix. With only two longitudinal velocities, the longitudinal position of the solute defines the amount of time spent in the fracture and matrix, because in the absence of longitudinal dispersion/diffusion, this location is given by

$$v_f t_f + v_{mz}(t - t_f) = z' \quad (67)$$

where t_f is the time spent in the fracture.

[60] Consider the dispersion/diffusion coefficient for any particular solute particle path starting at $z = 0$ and $t = 0$ and ending at $z = z'$ in the absence of longitudinal dispersion/diffusion. The dispersion/diffusion coefficient is a function of time that varies in response to solute movement between the fracture and matrix as a result of transverse advection and diffusion Therefore, the longitudinal diffusion/dispersion process is described by

$$\frac{\partial \tilde{c}}{\partial t} = D^*(t; z') \frac{\partial^2 \tilde{c}}{\partial z^2} \tag{68}$$

[61] This equation has the following fundamental solution:

$$\tilde{c}(z, t; z') = \frac{1}{\sqrt{4\pi \overline{D^*}(t, z')t}} \exp\left\{-\frac{z^2}{4\overline{D^*}(t, z')t}\right\} \tag{69}$$

where the time-averaged longitudinal diffusion/dispersion coefficient is

$$\overline{D^*}(t; z') = \frac{1}{t}\left\{D_f^* t_f + D_m^*(t - t_f)\right\} \tag{70}$$

and D_f^* is the longitudinal dispersion coefficient for the fracture divided the fracture retardation factor. Using equation (67) to solve for t_f, the time-averaged longitudinal diffusion/dispersion coefficient in (70) can be put in dimensionless form:

$$\overline{D_r^*}(\tau; \xi') = 1 + \left(D_{fm}^* - 1\right)\frac{\xi'}{\tau} \tag{71}$$

where $\overline{D_r^*} = \overline{D^*}/D_m^*$ and $D_{fm}^* = D_f^*/D_m^*$. The fact that solute concentrations for ξ' near τ tend to zero as $\tau \to \infty$ in equations (58) and (59) means that the effects of longitudinal dispersion in the fracture tend to diminish at longer times. This is a reflection of the fact that solute spreading into the matrix leads to a decreasing level of solute interaction with the fracture over time. The solute concentration including variable diffusion and dispersion between matrix and fracture is

$$\mathbb{C}_{mdk}(z, x, t) = \int_{v_{mz}t}^{v_f t} \frac{c_{mdk}\left(\frac{z' - v_{mz}t}{\ell}, \frac{x}{\ell}, \frac{v_f^* t}{\ell}\right)}{\sqrt{4\pi \overline{D^*}(t; z')t}} \exp\left\{-\frac{(z - z')^2}{4\overline{D^*}(t; z')t}\right\} dz' \tag{72}$$

or, in dimensionless form,

$$\mathbb{C}_{mdk}(\xi, \eta, \tau) = \int_0^{\tau} c_{mdk}(\xi', \eta, \tau) \frac{\sqrt{Pe}}{\sqrt{4\pi \overline{D_r^*}(\tau; \xi')\tau}} \exp\left\{-\frac{Pe(\xi - \xi')^2}{4\overline{D_r^*}(\tau; \xi')\tau}\right\} d\xi' \tag{73}$$

[62] This result has been derived for isotropic diffusion in the matrix. If the material is inherently anisotropic or if flow rates are sufficiently large to result in matrix dispersion, the diffusion or dispersion process will be anisotropic. If a principal axis of the material anisotropy or the overall matrix flow direction is parallel (or orthogonal) to the fracture, then the principal axes for the dispersion or diffusion processes are also in these directions. For these situations, longitudinal and transverse dispersion are independent processes and can be incorporated into the transport solution in the same way. The system analyzed by *Roubinet et al*. [2012] also had one of the principal axes of the diffusion process line up in the longitudinal (fracture) direction, with the other principal axis lining up in the orthogonal (transverse) direction. The case of a general orientation of the principal axes relative to the fracture results in transverse and longitudinal matrix diffusion/dispersion processes that are not independent; therefore, the superposition method presented here for incorporating longitudinal diffusion and dispersion is not applicable.

[63] Equation (73) was used to solve a problem that could be compared with an existing solution by *Tang et al*. [1981] that includes longitudinal dispersion in the fracture. The problem includes advection and dispersion in the fracture and lateral diffusion in the rock matrix, but does not include advection or longitudinal diffusion in the matrix. The assumption that solute is well mixed in the fracture cross section is also used. The *Tang et al*. [1981] solution was derived by directly solving the differential equations including longitudinal dispersion in the fracture. The problem solved by *Tang et al*. [1981] has a fixed concentration in the fracture at $z = 0$ for $t > 0$ and an initial concentration of zero in the fracture and matrix for $z > 0$. An equivalent initial value problem was constructed using a finite series of instantaneous point sources evenly spaced in the fracture along the negative z axis. The concentration evolution from each point source is given by equation (73). These concentrations are then linearly superimposed (summed) to generate the overall solution. The parameters of the problem are given in Figure 10. For these parameters, 150 instantaneous point sources, spaced 0.5 m starting at $z = -0.5$ m, were found to provide sufficient accuracy. The mass released at each source was determined by adjusting the 150 source masses such that the concentrations at $z = 0$ remained close to a constant value, c_0, for 2000 evenly spaced times over a

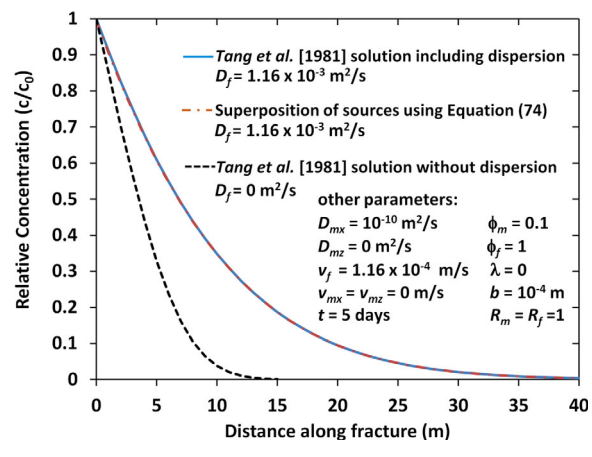

Figure 10. Exact solution including longitudinal dispersion for fracture concentration from *Tang et al*. [1981] compared with the superposition of instantaneous point-source solutions using equation (73); *Tang et al*. [1981] solution without dispersion is also shown.

Table 4. Fracture Longitudinal Dispersion Coefficients[a]

Case	7 and 10	8 and 11	9 and 12
Fracture longitudinal dispersion coefficient (m^2/s)	7×10^{-8}	1.16×10^{-4}	1.16×10^{-3}

[a]A longitudinal matrix diffusion coefficient of 10^{-10} m^2/s is used for Cases 7–12. All other parameters for Cases 7–9 are the same as for Case 1 and Cases 10–12 have the same parameters as Case 4. See Tables 2 and 3.

5 day period. This resulted in a root-mean square difference of 0.0035 between the 2000 computed relative concentrations, c/c_0, at $z = 0$ and the target value of 1. Figure 10 shows the comparison of fracture concentrations computed using solutions based on *Tang et al.* [1981], both including longitudinal dispersion in the fracture and without longitudinal dispersion ($D_f = 0$), and the superposition of solutions including longitudinal dispersion based on equation (73). The solution without longitudinal dispersion is included in the figure to show the effects of longitudinal dispersion on the solution. These comparisons show that the effects of longitudinal dispersion in this case are significant, and that the proposed method for introducing longitudinal dispersion into the solution matches the *Tang et al.* [1981] solution.

[64] The formulation for cumulative-mass arrivals including longitudinal dispersion/diffusion is given in the section A3.

6. Solution Behavior Including Longitudinal Diffusion/Dispersion

[65] An estimate of longitudinal dispersion within a fracture for the configuration in this model may be derived from the method for analyzing shear dispersion developed by *Taylor* [1953, 1954] and *Aris* [1956]. The result for the asymptotic shear dispersion coefficient for solute transport between parallel plates is [*Wooding*, 1960]

$$D_f^* = D_{f0}^* + \frac{1}{210}\frac{v_f^2 b^2}{D_{f0}^*} \tag{74}$$

where D_{f0}^* is the molecular diffusion coefficient in the fracture divided by the fracture retardation factor. Assuming $D_{f0}^* = D_m^*$, and using values for the parameters from Case 1 discussed in section 4, gives $D_f^* = 6.5 \times 10^{-9} m^2/s$, which is less than 2 orders of magnitude larger than the molecular diffusion coefficient, $D_m^* = 10^{-10} m^2/s$. *Zhou et al.* [2007] evaluated dispersion data from field-test results for both fracture networks and single fractures. Results on solute transport and dispersion for six single-fracture tests were documented. Their findings indicated that dispersion in a real (single) fracture is typically more than 2 orders of magnitude larger than for flow between parallel plates. This is believed to be a result of fracture surface roughness and spatial heterogeneity of the fracture aperture. The tests for single fractures were found to have dispersivities ranging from 0.18 to 2.4 m and dispersion coefficients

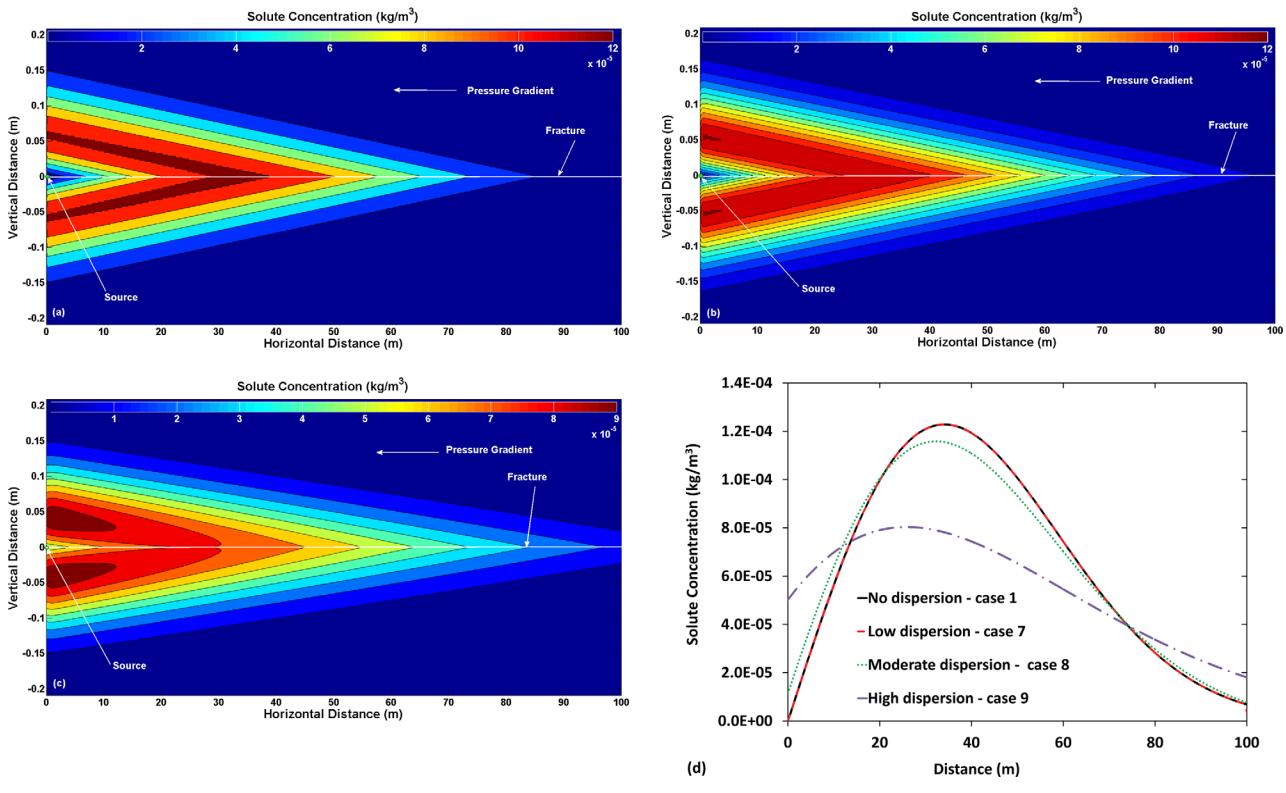

Figure 11. Cases 7–9: Concentration contours at 200 days using Case 1 parameters but with a matrix longitudinal diffusion coefficient of 10^{-10} m^2/s and fracture longitudinal dispersion coefficient of (a) 7×10^{-8} m^2/s; (b) 1.16×10^{-4} m^2/s; (c) 1.16×10^{-3} m^2/s; (d) centerline concentration profiles for Cases 1 and 7–9.

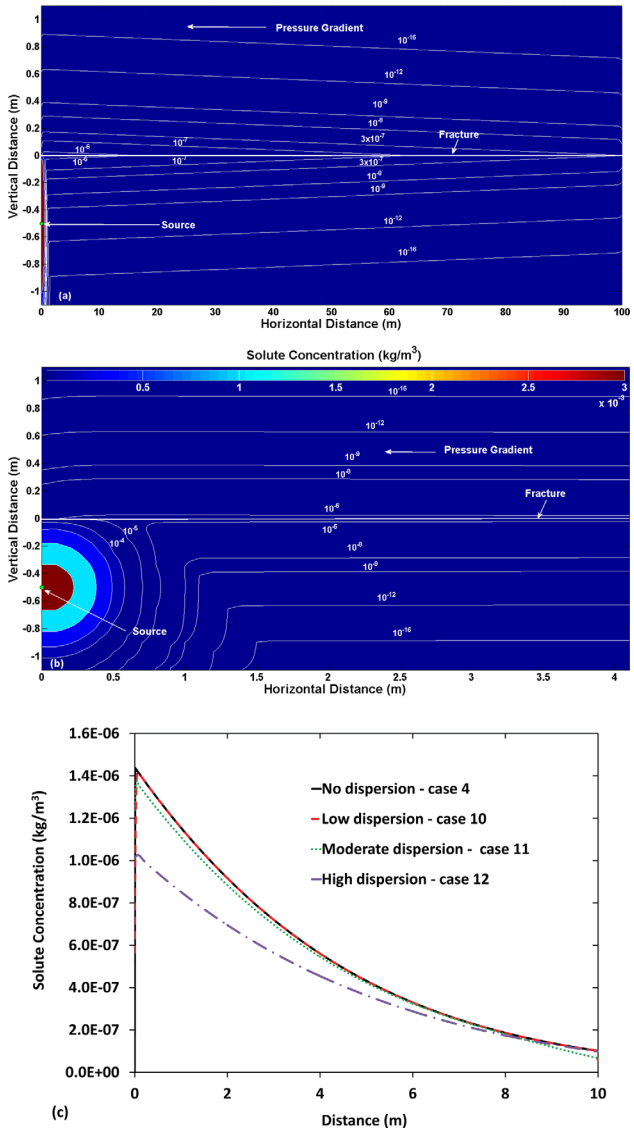

Figure 12. Case 10: Concentration contours at 2000 days using Case 4 parameters but with a matrix longitudinal diffusion coefficient of 10^{-10} m^2/s and fracture longitudinal dispersion coefficient of 7×10^{-8} m^2/s, (a) full-scale version; contour lines are marked with concentrations in kg/m^3; (b) detail of contours near the source; (c) centerline concentration profiles for Cases 4 and 10–12.

ranging from 2×10^{-5} to 8×10^{-4} m^2/s. We span this range by computing low, moderate, and high-dispersion cases as shown in Table 4. The two highest dispersion coefficients were selected such that fracture dispersivities (the ratio of the fracture dispersion coefficient to the fracture velocity) have values of 1 and 10 m, respectively. As will be seen, the higher levels of the dispersion coefficient are needed to show the effects of fracture dispersion in the results. Other parameters used for these calculations are given in Tables 2 and 3. Note that sorption (K_{df} and K_{dm}) coefficients and the decay constant (λ) are zero.

[66] Solutions including longitudinal dispersion in the fracture and longitudinal diffusion in the matrix are shown in Figures 11 and 12. Cases 7–9 are shown in Figure 11 and are equivalent to Case 1, but now include varying levels of longitudinal dispersion in the fracture and a fixed level of longitudinal diffusion in the matrix (10^{-10} m^2/s). Some additional longitudinal spreading can be seen in the profile in Figure 11a, also at 200 days, as compared with Figure 4a. At higher levels of longitudinal dispersion in the fracture in Figures 11b and 11c, the effects of dispersion on the concentration contours becomes more noticeable, and increased levels of solute movement upstream of the release point are also observed. While solute diffusion upstream of the release point can occur as a result of molecular diffusion, its enhancement as a result of higher levels of longitudinal dispersion is not physical. This occurs because longitudinal dispersion in the fracture is represented as a Fickian process, which is an approximation that becomes valid at long times. The fracture concentration profiles in Figure 11d show the similarity of the concentrations for no dispersion (Case 1) and low dispersion (Case 7), but deviates perceptibly for the moderate dispersion case (Case 8) and significantly for the high dispersion (Case 9).

[67] Cases 10–12 shown in Figure 12 are for a matrix-release initial condition and are the same as that shown in Case 4, except here, varying levels of longitudinal dispersion in the fracture and a fixed level of longitudinal diffusion in the matrix are included (10^{-10} m^2/s). Longitudinal diffusion in the matrix helps to reveal the behavior of solute that is in the matrix prior to interaction with the fracture. Most of the solute released has not interacted with the fracture, so the concentration profile in the matrix follows a fairly simple advection-diffusion pattern. The differences in concentration contours caused by changes in fracture dispersion coefficient are difficult to distinguish; therefore, only the contours for the low-dispersion case are shown in Figure 12a and an expanded view in Figure 12b near the source for 2000 days. As in Figure 11d, the centerline profile in Figure 12c shows virtually no difference between the no dispersion (Case 4) and low dispersion (Case 10), and only a modest difference for the moderate dispersion case (Case 11), but a noticeable change for the high dispersion (Case 12).

[68] For solute release in the matrix, solute that has not interacted with the fracture remains at $\xi = 0$ (the solute release location in a coordinate system moving at the matrix longitudinal velocity) unless longitudinal diffusion is included. *Roubinet et al.* [2012] have shown that at low Peclet numbers, longitudinal diffusion in the matrix can have a significant effect on solute transport through the fracture. For solute that has interacted with the fracture, differential advection caused by fracture-matrix interaction can overshadow other dispersion/diffusion processes, as shown here for the low fracture-dispersion case based on parallel-plate fracture geometry. Higher levels of longitudinal dispersion associated with natural fractures can lead to a more significant impact on the overall dispersion.

7. Evaluation of Longitudinal Diffusion and Dispersion

[69] To determine an approximate criterion for when longitudinal dispersion in the fracture becomes

important for the overall transport process, we first compute the integral of the concentrations in equations (58) and (59) over the transverse coordinate, which gives, respectively,

$$\int_0^\infty c_{mdo}(\xi,\eta,\tau)d\eta = \bar{c}_{mdo}(\xi,\tau) = \frac{H(\tau-\xi)H(\xi)}{2\sqrt{\pi}\sqrt{Pe}\sqrt{\tau-\xi}}\exp\left(-\frac{PeV_o\eta_0}{2}\right)\exp\left[-\frac{(\xi+Pe\eta_0)^2+Pe^2V^2(\tau-\xi)^2}{4Pe(\tau-\xi)}\right] -H(\tau-\xi)H(\xi)\frac{V_o}{4}\exp\left(\frac{V_o\xi}{2}\right)\mathrm{erfc}\left[\frac{\xi+Pe\eta_0+PeV_o(\tau-\xi)}{2\sqrt{Pe}\sqrt{\tau-\xi}}\right] \tag{75}$$

$$\int_0^\infty c_{mds}(\xi,\eta,\tau)d\eta = \bar{c}_{mds}(\xi,\tau) = \frac{H(\tau-\xi)H(\xi)}{2\sqrt{\pi}\sqrt{Pe}\sqrt{\tau-\xi}}\exp\left(\frac{PeV_s\eta_0}{2}\right)\exp\left(-\frac{(\xi+Pe\eta_0)^2+Pe^2V^2(\tau-\xi)^2}{4Pe(\tau-\xi)}\right) -H(\tau-\xi)H(\xi)\frac{V_s}{4}\exp\left(\frac{V_s\xi}{2}\right)\exp(PeV_s\eta_0)\mathrm{erfc}\left[\frac{\xi+Pe\eta_0+PeV_s(\tau-\xi)}{2\sqrt{Pe}\sqrt{\tau-\xi}}\right] \tag{76}$$

where the trailing spike on the source side is not included because this solute has not interacted with the fracture and is not dispersed longitudinally.

[70] Equations (75) and (76) are still complex, mainly as a result of the effects of cross-flow and source offset from the fracture. These factors affect the amount of spreading caused by fracture-matrix interaction, and they also have a similar affect on the amount of spreading caused by longitudinal dispersion in the fracture, because both are impacted mainly by the same delay in solute interaction with the fracture imposed by these conditions. Therefore, longitudinal spreading is evaluated for the simpler case with $\eta_0 = V_s = V_o = 0$. Then,

$$\bar{c}_{mdo}(\xi,\tau) = \bar{c}_{mds}(\xi,\tau) = \frac{H(\tau-\xi)H(\xi)}{2\sqrt{\pi}\sqrt{Pe}\sqrt{\tau-\xi}}\exp\left(-\frac{\xi^2}{4Pe(\tau-\xi)}\right) \tag{77}$$

[71] As τ increases, most of the solute mass lies at longitudinal positions where $\xi \ll \tau$ suggesting that $(\tau-\xi)\approx\tau$ giving

$$\bar{c}_{mdo}(\xi,\tau) = \bar{c}_{mds}(\xi,\tau) = \frac{H(\tau-\xi)H(\xi)}{2\sqrt{\pi}\sqrt{Pe}\sqrt{\tau}}\exp\left(-\frac{\xi^2}{4Pe\tau}\right) \tag{78}$$

[72] This shows that the form of the integrated solution is like diffusion from an instantaneous point source that originated at $\xi=0$, but the solution is truncated at $\xi=0$ and $\xi=\tau$. The standard deviation of the distribution as a dimensional quantity, not accounting for the truncation, is $\sqrt{2Pe\tau\ell^2}$. The truncation essentially represents a half space over which the spreading occurs, because the boundary at $\xi=\tau$ is relatively far removed from the main solute mass. As a result, one half of the standard deviation may be considered a length scale for the degree of longitudinal spreading induced by fracture-matrix interaction, which is, as a dimensional quantity,

$$S_{fm} \sim \frac{1}{2}\sqrt{2Pe\tau\ell^2} \tag{79}$$

[73] The spreading caused by longitudinal diffusion/dispersion is given by $\sqrt{2\overline{\overline{D^*}}t}$, where $\overline{\overline{D^*}}$ is the solute-mass weighted average of $\overline{D^*}$:

$$\overline{\overline{D^*}}(\tau) = \int_0^\tau \frac{\overline{D^*}(\tau,\ \xi)}{2\sqrt{\pi}\sqrt{Pe}\sqrt{\tau}}\exp\left(-\frac{\xi^2}{4Pe\tau}\right)d\xi \tag{80}$$

[74] The solute-mass concentration distribution used for the average in (80) is the approximate distribution given by (78). Integrating (80) using equation (70) for $\overline{D^*}(\tau,\ \xi)$ gives

$$\overline{\overline{D^*}}(\tau) = \frac{D_m^*}{2}\mathrm{erf}\left(\sqrt{\frac{\tau}{4Pe}}\right) + \frac{D_f^*-D_m^*}{\sqrt{\pi}}\sqrt{\frac{Pe}{\tau}}\left\{1-\exp\left(-\frac{\tau}{4Pe}\right)\right\} \tag{81}$$

[75] The comparable longitudinal spreading caused by dispersion and diffusion is

$$S_{disp-dif} \sim \sqrt{2\overline{\overline{D^*}}(\tau)t} \tag{82}$$

[76] Therefore, an approximate criterion for when longitudinal diffusion and dispersion in the fracture and matrix are small relative to spreading caused by fracture-matrix differential advection is when S_{fm} in (79) is large compared with $S_{disp-dif}$ in (82). Using equations (79), (81), and (82), and stipulating that $S_{disp-dif} < S_{fm}$, gives:

$$\beta\sqrt{D_m^*\mathrm{erf}\left(\sqrt{\frac{\tau}{4Pe}}\right)t + \frac{2\left(D_f^*-D_m^*\right)t}{\sqrt{\pi}}\sqrt{\frac{Pe}{\tau}}\left\{1-\exp\left(-\frac{\tau}{4Pe}\right)\right\}} < \frac{1}{2}\sqrt{2Pe\tau\ell^2} \tag{83}$$

where β is a factor to be determined.

[77] Putting equation (83) entirely in terms of nondimensional variables gives

$$\Omega = \frac{2\beta^2}{Pe^2}\left[\mathrm{erf}\left(\sqrt{\frac{\tau}{4Pe}}\right) + \frac{D_{fm}^*-1}{\sqrt{\pi}}\sqrt{\frac{4Pe}{\tau}}\left\{1-\exp\left(-\frac{\tau}{4Pe}\right)\right\}\right] < 1 \tag{84}$$

[78] Equation (84) indicates that fracture-matrix interaction dominates longitudinal spreading if $\Omega < 1$ The value of Ω is strongly influenced by the Peclet number and the ratio of the fracture longitudinal dispersion coefficient to the matrix diffusion coefficient, with somewhat weaker dependence on time. The value of β represents the ratio of longitudinal spreading length scales associated with fracture-matrix interaction and matrix diffusion/fracture dispersion, such that fracture-matrix interaction dominates longitudinal spreading. Conceptually, this is expected to be greater than 1 but probably less than 10; therefore, β is assigned a value of 3. With this choice, the values of Ω are 0.0014, 0.86, and 48.4 for the low, moderate, and high

longitudinal dispersion cases in Figure 11d, respectively. For the low, moderate, and high longitudinal dispersion cases in Figure 12c, Ω is 0.0045, 0.27, and 2.7, respectively. The values of Ω are smaller for corresponding low, moderate, and high-dispersion cases in Figure 12c as compared with Figure 11d because the value of τ is an order of magnitude larger for Figure 12c as compared with Figure 11d. These values of Ω indicate that longitudinal dispersion and diffusion should have negligible effects on longitudinal spreading for cases 7 and 10, which use the low longitudinal dispersion coefficient, a minor effect for Case 8, and an even smaller effect for Case 11, both of which use the moderate longitudinal dispersion coefficient; and significant effects for Cases 9 and 12, where the high longitudinal dispersion coefficient is used.

[79] *Roubinet et al*. [2012] investigated the effects of longitudinal diffusion in the matrix on transport for an instantaneous point source and computed three cases for different Peclet numbers. They found that longitudinal matrix diffusion effects are less significant as the Peclet number increases [*Roubinet et al*., 2012]. Application of equation (84) to these cases gives values of $\Omega$of 0.2, 0.8, and 20 for high, middle, and low-Peclet number cases, respectively. These values of Ω are consistent with the responses found by *Roubinet et al*. [2012, Figure 5], which show almost no effect of longitudinal-matrix diffusion for the high-Peclet number case, a small but distinct effect for the middle-Peclet number case, and a significant effect for the low-Peclet number case.

8. Conclusions

[80] We have developed a mathematical model for two-dimensional flow and transport through a water-saturated single fracture and permeable rock matrix for which analytical solutions have been obtained. This model incorporates several factors not included in existing analytical solutions for this kind of transport problem. The new model capabilities are (1) two-dimensional flow in the matrix with an arbitrary flow direction relative to the fracture orientation, (2) a general solute source-release point that can be either in the fracture or matrix, and (3) independent longitudinal dispersion and diffusion in the fracture and matrix, respectively. A closed-form analytical solution was obtained for two-dimensional solute concentration if longitudinal dispersion and diffusion could be neglected. Some example calculations show that significant delay in radionuclide transport can occur as a result of an offset of the source location from the fracture or as a result of matrix cross-flow. We then developed a method for incorporating the effects of longitudinal dispersion in the fracture and longitudinal diffusion in the matrix. The resulting solution including these mechanisms takes the form of a superposition integral. A closed-form analytical solution is used to develop an approximate criterion to evaluate conditions in which longitudinal dispersion in the fracture and longitudinal diffusion in the matrix are expected to be significant, relative to longitudinal spreading caused by fracture-matrix interaction. The significance of longitudinal dispersion in the fracture and longitudinal diffusion in the matrix has been shown to be a strong function of Peclet number, with the influence of these processes decreasing as Peclet number increases. The effects of fracture longitudinal dispersion also diminish with the ratio of fracture longitudinal dispersion coefficient to matrix diffusion coefficient. The new transport solutions presented here are valuable for checking the influence of the various advective and diffusive processes on transport through a rock fracture and matrix when matrix advective transport is not negligible, and can be used to verify the ability of numerical simulations to capture these transport processes.

[81] Solute transport cases analyzed with the analytical model show that matrix cross-flow has an increasing effect on solute transport, as the orientation of the fracture relative to the hydraulic gradient goes from parallel to orthogonal. This is a result of increasing cross-flow and decreasing flow along the fracture. The effects of cross-flow result in reduced solute interaction with the fracture, such that a greater degree of longitudinal advance of solute occurs in the matrix. As the effects of cross-flow become stronger, more of the solute transport occurs in the matrix, and transport times approach the time for advection through the matrix. Significant delays in transport can also occur for cases in which solute is released into the matrix, with the main impact found on the early breakthrough behavior and the secondary impact on the trailing portion of the breakthrough.

Appendix A: Results for Cumulative Arrivals at a Downstream Location From an Instantaneous Point Source

A1. Cumulative Arrivals Neglecting Longitudinal Diffusion/Dispersion

[82] The results for concentrations obtained in section 3 can be integrated at a position downstream along the fracture for cumulative-mass arrivals in the fracture, M_f, and on both sides of the matrix, M_k. The procedure for the cumulative mass integration is the same as reported in *Houseworth* [2006].

[83] The cumulative-mass arrival in the fracture at a location z_ℓ along the fracture axis is given by

$$M_f(T) = \int_0^T A_f \phi_f R_f v_f c_f(z_e, t) dt \tag{A1}$$

[84] Putting this into dimensionless form gives

$$\frac{M_f(\psi)}{M_0} = 2 \int_0^\psi c_{fd}(\zeta_e - V_\ell \sigma, (1 - V_\ell)\sigma) \exp(-\lambda_d \sigma) d\sigma \tag{A2}$$

[85] For the cumulative mass solutions, the following additional dimensionless variables are defined: $V_\ell = v_{mz}/v_f$, $\zeta_e = z_e/\ell$, $\lambda_d = \lambda\ell/v_f$, $\psi = v_f T/\ell$, $\sigma = v_f t/\ell$, where z_e is the downstream location at which cumulative-mass arrivals are computed and T is the time of observation at z_e. The result for cumulative-mass arrival in the fracture is:

$$\begin{aligned}\frac{M_f(\psi)}{M_0} &= \frac{\sqrt{V_\ell^2 + Pe^2V^2 + 4Pe\lambda_d} + V_\ell}{2\sqrt{V_\ell^2 + Pe^2V^2 + 4Pe\lambda_d}} \\ &\times\exp\left(\frac{\{\zeta_e(1-V_\ell) + Pe\eta_0\}\left\{\sqrt{V_\ell^2 + Pe^2V^2 + 4Pe\lambda_d} + V_\ell\right\} - 2Pe\lambda_d\zeta_e}{2Pe} - \frac{PeV_s\eta_0}{2}\right) \\ &\times\mathrm{erfc}\left(\frac{\{\zeta_e(1-V_\ell) + Pe\eta_0\}}{2\sqrt{Pe}\sqrt{\psi-\zeta_e}} + \frac{\sqrt{V_\ell^2 + Pe^2V^2 + 4Pe\lambda_d}\sqrt{\psi-\zeta_e}}{2\sqrt{Pe}}\right) \\ &+ \frac{\sqrt{V_\ell^2 + Pe^2V^2 + 4Pe\lambda_d} - V_\ell}{2\sqrt{V_\ell^2 + Pe^2V^2 + 4Pe\lambda_d}} \\ &\times\exp\left(-\frac{\{\zeta_e(1-V_\ell) + Pe\eta_0\}\left\{\sqrt{V_\ell^2 + Pe^2V^2 + 4Pe\lambda_d} - V_\ell\right\} + 2Pe\lambda_d\zeta_e}{2Pe} - \frac{PeV_s\eta_0}{2}\right) \\ &\times\mathrm{erfc}\left(\frac{\{\zeta_e(1-V_\ell) + Pe\eta_0\}}{2\sqrt{Pe}\sqrt{\psi-\zeta_e}} - \frac{\sqrt{V_\ell^2 + Pe^2V^2 + 4Pe\lambda_d}\sqrt{\psi-\zeta_e}}{2\sqrt{Pe}}\right)\end{aligned} \tag{A3}$$

[86] The cumulative-mass arrival in the downstream matrix at a boundary passing through z_e on the fracture axis is given by

$$M_{mk}(T) = \int_0^T \int_0^\infty \frac{A_f}{b}\phi_m R_m v_{mz} c_{mk}(z_e, x, t)\,dx\,dt \tag{A4}$$

[87] Putting this into dimensionless form gives

$$\frac{M_{mk}(\psi)}{M_0} = V_\ell \int_0^\psi \int_0^\infty c_{mdk}(\zeta_e - V_\ell\sigma, \eta, (1-V_\ell)\sigma)\exp(-\lambda_d\sigma)\,d\eta\,d\sigma \tag{A5}$$

[88] The result for cumulative-mass arrival in matrix on opposite side of fracture from the source release location is:

$$\begin{aligned}\frac{M_{mo}(\psi)}{M_0} &= \frac{V_\ell V_s}{2(V_sV_\ell + 2\lambda_d)}\exp\left(-\frac{(V_sV_\ell + 2\lambda_d)(\psi-\zeta_e) - V_s(1-V_\ell)\zeta_e + 2\lambda_d\zeta_e}{2}\right) \\ &\times\mathrm{erfc}\left\{\frac{\{\zeta_e(1-V_\ell) + Pe\eta_0\} + (PeV_s - V_\ell)(\psi-\zeta_e)}{2\sqrt{Pe}\sqrt{\psi-\zeta_e}}\right\} \\ &- \left\{\frac{V_\ell V_s(PeV_s - V_\ell) + V_\ell V_s\sqrt{Pe^2V^2 + V_\ell^2 + 4Pe\lambda_d}}{4(V_sV_\ell + 2\lambda_d)\sqrt{Pe^2V^2 + V_\ell^2 + 4Pe\lambda_d}} + \frac{V_\ell}{2\sqrt{Pe^2V^2 + V_\ell^2 + 4Pe\lambda_d}}\right\} \\ &\times\exp\left(\frac{\{\zeta_e(1-V_\ell) + Pe\eta_0\}\left\{\sqrt{Pe^2V^2 + V_\ell^2 + 4Pe\lambda_d} + V_\ell\right\} - 2Pe\lambda_d\zeta_e}{2Pe} - PeV_s\eta_0\right) \\ &\times\mathrm{erfc}\left(\frac{\{\zeta_e(1-V_\ell) + Pe\eta_0\} + (\psi-\zeta_e)\sqrt{Pe^2V^2 + V_\ell^2 + 4Pe\lambda_d}}{2\sqrt{Pe}\sqrt{\psi-\zeta_e}}\right) \\ &+ \left\{\frac{V_\ell V_s(PeV_s - V_\ell) - V_\ell V_s\sqrt{Pe^2V^2 + V_\ell^2 + 4Pe\lambda_d}}{4(V_oV_\ell + 2\lambda_d)\sqrt{Pe^2V^2 + V_\ell^2 + 4Pe\lambda_d}} + \frac{V_\ell}{2\sqrt{Pe^2V^2 + V_\ell^2 + 4Pe\lambda_d}}\right\} \\ &\times\exp\left(-\frac{\{\zeta_e(1-V_\ell) + Pe\eta_0\}\left\{\sqrt{Pe^2V^2 + V_\ell^2 + 4Pe\lambda_d} - V_\ell\right\} + 2Pe\lambda_d\zeta_e}{2Pe} - PeV_s\eta_0\right) \\ &\times\mathrm{erfc}\left(\frac{\{\zeta_e(1-V_\ell) + Pe\eta_0\} - (\psi-\zeta_e)\sqrt{Pe^2V^2 + V_\ell^2 + 4Pe\lambda_d}}{2\sqrt{Pe}\sqrt{\psi-\zeta_e}}\right)\end{aligned} \tag{A6}$$

[89] The cumulative-mass arrival in matrix on same side of fracture as the source release location is:

$$
\begin{aligned}
\frac{M_{ms}(\psi)}{M_0} = {} & \frac{V_\ell V_s}{2(V_s V_\ell - 2\lambda_d)} \exp\left(\frac{(V_s V_\ell - 2\lambda_d)(\psi - \zeta_e) - V_s(1 - V_\ell)\zeta_e - 2PeV_s\eta_0 - 2\lambda_d\zeta_e}{2}\right) \\
& \times \mathrm{erfc}\left\{\frac{\{\zeta_e(1 - V_\ell) + Pe\eta_0\} - (PeV + V_\ell)(\psi - \zeta_e)}{2\sqrt{Pe}\sqrt{\psi - \zeta_e}}\right\} \\
& + \left\{\frac{V_\ell V_s(PeV_s + V_\ell) - V_\ell V_s\sqrt{Pe^2V^2 + V_\ell^2 + 4Pe\lambda_d}}{4(V_s V_\ell - 2\lambda_d)\sqrt{Pe^2V^2 + V_\ell^2 + 4Pe\lambda_d}} - \frac{V_\ell}{2\sqrt{Pe^2V^2 + V_\ell^2 + 4Pe\lambda_d}}\right\} \\
& \times \exp\left(\frac{\{\zeta_e(1 - V_\ell) + Pe\eta_0\}\left\{\sqrt{Pe^2V^2 + V_\ell^2 + 4Pe\lambda_d} + V_\ell\right\} - 2Pe\lambda_d\zeta_e}{2Pe} - \frac{PeV_s\eta_0}{2}\right) \\
& \times \mathrm{erfc}\left(\frac{\{\zeta_e(1 - V_\ell) + Pe\eta_0\} + (\psi - \zeta_e)\sqrt{Pe^2V^2 + V_\ell^2 + 4Pe\lambda_d}}{2\sqrt{Pe}\sqrt{\psi - \zeta_e}}\right) \\
& - \left\{\frac{V_\ell V_s(PeV_s + V_\ell) + V_\ell V_s\sqrt{Pe^2V^2 + V_\ell^2 + 4Pe\lambda_d}}{4(V_s V_\ell - 2\lambda_d)\sqrt{Pe^2V^2 + V_\ell^2 + 4Pe\lambda_d}} - \frac{V_\ell}{2\sqrt{Pe^2V^2 + V_\ell^2 + 4Pe\lambda_d}}\right\} \\
& \times \exp\left(-\frac{\{\zeta_e(1 - V_\ell) + Pe\eta_0\}\left\{\sqrt{Pe^2V^2 + V_\ell^2 + 4Pe\lambda_d} - V_\ell\right\} + 2Pe\lambda_d\zeta_e}{2Pe} - \frac{PeV_s\eta_0}{2}\right) \\
& \times \mathrm{erfc}\left(\frac{\{\zeta_e(1 - V_\ell) + Pe\eta_0\} - (\psi - \zeta_e)\sqrt{Pe^2V^2 + V_\ell^2 + 4Pe\lambda_d}}{2\sqrt{Pe}\sqrt{\psi - \zeta_e}}\right) \\
& + \frac{1}{2}H(V_\ell\psi - \zeta_e)\left[1 + \mathrm{erf}\left\{\frac{\sqrt{Pe}(\eta_0 + V_s(1 - V_\ell)\psi)}{2\sqrt{(1 - V_\ell)\psi}}\right\}\right] \\
& - \frac{1}{2}H(V_\ell\psi - \zeta_e)\exp(-PeV_s\eta_0)\mathrm{erfc}\left\{\frac{\sqrt{Pe}(\eta_0 - V_s(1 - V_\ell)\psi)}{2\sqrt{(1 - V_\ell)\psi}}\right\}
\end{aligned}
\tag{A7}
$$

where the term involving the step function represents the arrival of solute mass in the matrix that did not interact with the fracture.

A2. Relationship Between the Solution for Concentration From a Constant-Rate Continuous Source and the Cumulative Mass Solution for an Instantaneous Point Source for Cases With No Longitudinal Diffusion or Dispersion

[90] The cumulative mass solutions in section A1 are related to the concentration from a constant-rate continuous source. This is demonstrated here for a source release in the fracture. Starting with equation (A1), we assign a Green's function, $g_f(z_e, t)$, for the fracture cumulative mass equation through the relationship $c_f(z_e, t) = M_0 g_f(z_e, t)$, giving

$$\frac{M_f(T)}{M_0} = A_f\phi_f R_f v_f \int_0^T g_f(z_e, t)dt \tag{A8}$$

[91] The concentration from a continuous source solution for a boundary concentration of c_0 can be written as a superposition integral for a constant-rate mass release $\dot{M}$ at the origin,

$$c_f = \dot{M}\int_0^T g_f(z_e, T - \sigma)d\sigma = \dot{M}\int_0^T g_f(z_e, t)dt \tag{A9}$$

[92] The mass release rate equals the advective mass flux at a concentration of c_0:

$$\dot{M} = A_f\phi_f R_f v_f c_0 \tag{A10}$$

[93] Therefore,

$$\frac{c_f}{c_0} = \frac{M_f(T)}{M_0} = A_f\phi_f R_f v_f \int_0^T g_f(z_e, \tau)d\tau \tag{A11}$$

[94] Based on equation (A11), when $V_\ell = V = \eta_0 = 0$, equation (A3) reduces to *Tang et al.* [1981, equation (42)] for concentration in the fracture from a continuous source.

[95] For the matrix, we assign a Green's function $c_{mk}(z_e, x, t) = M_0 g_m(z_e, x, t)$ and use it in equation (A4) to yield,

$$\frac{M_{mk}(T)}{M_0} = \int_0^T\int_0^\infty \frac{A_f}{b}\phi_m R_m v_{mz} g(z_e, x, t)dxdt \tag{A12}$$

[96] Simplifying equation (A12) gives

$$\frac{2\ell M_{mk}(T)}{M_0 V_\ell} = A_f \phi_f R_f v_f \int_0^T \int_0^\infty g(z_e, x, t) dx dt \tag{A13}$$

[97] As for the fracture, the continuous source solution at a concentration of c_0 can be written as a superposition integral for a constant-rate mass release $\dot{M}$ at the origin:

$$\begin{aligned}\int_0^\infty c_m dx &= \dot{M} \int_0^T \int_0^\infty g_m(z_e, x, T-\sigma) dx d\sigma \\ &= \dot{M} \int_0^T \int_0^\infty g_m(z_e, x, t) dx dt \end{aligned} \tag{A14}$$

[98] Using (A10) for $\dot{M}$ gives

$$\int_0^\infty \frac{c_m}{c_0} dx = \frac{2\ell M_{mk}(T)}{M_0 V_\ell} = A_f \phi_f R_f v_f \int_0^T \int_0^\infty g_m(z_e, x, t) dx dt \tag{A15}$$

[99] Based on equation (A15), when $V_\ell = V_s = \eta_0 = 0$, the expression for $2\ell M_{mk}(T)/(M_0 V_\ell)$ using equations (A6) or (A7) gives the same result as found when the solution given by *Tang et al*. [1981, equation (44)] is integrated over the lateral direction (x) from b to ∞. Note that for *Tang et al*. [1981], the integral of c_m/c_0 goes from b to ∞ (in the notation of *Tang et al*. [1981]) rather than from 0 to ∞, because the origin for the transverse coordinate is at the center of the fracture. Also, b in *Tang et al*. [1981] notation is the fracture half-aperture; in this paper, b is the fracture aperture.

A3. Cumulative Arrivals Including Longitudinal Diffusion/Dispersion

[100] Cumulative arrivals at a downstream location including dispersion/diffusion result from advective and diffusive/dispersive transport. Therefore, equations (A1) and (A4) must be modified as follows:

$$\begin{aligned} M_f(T) = &\int_0^T A_f \phi_f R_f v_f \mathbb{C}_{mk}(z_e, 0, t) dt \\ &+ \int_0^T A_f \phi_f R_f D_f^* \frac{\partial \mathbb{C}_{mk}(z, 0, t)}{\partial z}\Big|_{z_e} dt \end{aligned} \tag{A16}$$

$$\begin{aligned} M_{mk}(T) = &\int_0^T \int_0^\infty \frac{A_f}{b} \phi_m R_m v_{mz} \mathbb{C}_{mk}(z_e, x, t) dx dt \\ &+ \int_0^T \int_0^\infty \frac{A_f}{b} \phi_m R_m D_m^* \frac{\partial \mathbb{C}_{mk}(z, x, t)}{\partial z}\Big|_{z_e} dx dt. \end{aligned} \tag{A17}$$

where $\mathbb{C}_{mk}(z, x, t)$ is the dimensional form of concentration corresponding to equation (72), accounting for longitudinal dispersion in the fracture and longitudinal diffusion in the matrix.

[101] The first terms in equations (A16) and (A17) account for longitudinal advective transport; the second terms are for longitudinal dispersive and diffusive transport. These may be put into dimensionless form:

$$\begin{aligned} \frac{M_f(\psi)}{M_0} = &\sqrt{\frac{Pe}{\pi}} \int_0^\psi \exp(-\lambda_d \sigma) \int_{V_\ell \sigma}^\sigma \left\{ \frac{D_{fm}^*(\zeta' - V_\ell \sigma) + (\sigma - \zeta') + D_{fm}^* \left(\frac{1 - V_\ell}{2}\right)(\zeta_e - \zeta')}{\left\{D_{fm}^*(\zeta' - V_\ell \sigma) + (\sigma - \zeta')\right\}^{3/2}} \right\} \\ &\times \exp\left\{ -\frac{Pe(\zeta_e - \zeta')^2}{4D_{fm}^*(\zeta' - V_\ell \sigma) + 4(\sigma - \zeta')} \right\} c_{fd}(\zeta' - V_\ell \sigma, (1 - V_\ell)\sigma) d\zeta' d\sigma \end{aligned} \tag{A18}$$

$$\begin{aligned} \frac{M_{mk}(\psi)}{M_0} = &\frac{V_\ell}{2} \sqrt{\frac{Pe}{\pi}} \int_0^\psi \exp(-\lambda_d \sigma) \int_{V_\ell \sigma}^\sigma \frac{D_{fm}^*(\zeta' - V_\ell \sigma) + (\sigma - \zeta') + \left(\frac{1 - V_\ell}{2V_\ell}\right)(\zeta_e - \zeta')}{\left\{D_{fm}^*(\zeta' - V_\ell \sigma) + (\sigma - \zeta')\right\}^{3/2}} \\ &\times \exp\left\{ -\frac{Pe(\zeta_e - \zeta')^2}{4D_{fm}^*(\zeta' - V_\ell \sigma) + 4(\sigma - \zeta')} \right\} \left\{ \int_0^\infty c_{mdk}(\zeta' - V_\ell \sigma, \eta, (1 - V_\ell)\sigma) d\eta \right\} d\zeta' d\sigma \end{aligned} \tag{A19}$$

[102] The integral over η in the matrix cumulative-mass-arrival formula can be reduced analytically, but is left here in the integral form.

[103] **Acknowledgments.** We thank Abdulla Cihan and Dan Hawkes at LBNL for their careful reviews of a draft manuscript. Funding for this work was provided by the Used Fuel Disposition Campaign, Office of Nuclear Energy, of the U.S. Department of Energy under contract DE-AC02-05CH11231 with Berkeley Lab.

References

Aris, R. (1956), On the dispersion of a solute in a fluid flowing through a tube, *Proc. R. Soc. London, Ser. A*, *235*, 67–77.

Bear, J. (1972), *Dynamics of Fluids in Porous Media*, Elsevier, New York.

Berkowitz, B. (2002), Characterizing flow and transport in fractured geological media: A review, *Adv. Water Resour.*, *25*, 861–884.

Birkhölzer, J., and G. Rouve (1994), Dual-continuum modeling of contaminant transport in fractured formations, paper presented at Tenth International Conference on Computational Methods in Water Resources, Heidelberg, Germany, Interdisziplinäres Zentrum für Wissenschaftliches

Rechnen (Interdisciplinary Center for Scientific Computing) and Sonderforschungsbereich 359 of Heidelberg University and the Institute of Supercomputing and Applied Mathematics of IBM Heidelberg, Germany.

Birkhö1zer, J., H. Rubin, H. Daniels, and G. Rouvé (1993a), Contaminant advection and spreading in a fractured permeable formation: Part 1. Parametric evaluation and analytical solution, *J. Hydrol.*, *144*, 1–33.

Birkhö1zer, J., H. Rubin, H. Daniels, and G. Rouvé (1993b), Contaminant advection and spreading in a fractured permeable formation: Part 2. Numerical simiulation, *J. Hydrol.*, *144*, 35–58.

Birkholzer, J., J. Houseworth, and C.-F. Tsang (2012), Geologic disposal of high-level radioactive waste—Status, key issues, and trends, *Annu. Rev. Environ. Resour.*, *37*, 79–106, doi:10.1146/annurev-environ-090611–143314.

Bodin, J., F. Delay, and G. de Marsily (2003a), Solute transport in a single fracture with negligible matrix permeability: 1. Fundamental mechanisms, *Hydrogeol. J.*, *11*, 418–433, doi:10.1007/s10040-003-0268-2.

Bodin, J., F. Delay, and G. de Marsily (2003b), Solute transport in a single fracture with negligible matrix permeability: 2. Mathematical formalism, *Hydrogeol. J.*, *11*, 434–454, doi:10.1007/s10040-003-0269-1.

Carslaw, H. S., and J. C. Jaeger (1959), *Conduction of Heat in Solids*, 2nd ed., Oxford Univ. Press, New York.

Cihan, A., and J. S. Tyner (2011), 2-D radial analytical solutions for solute transport in a dual-porosity medium, *Water Resour. Res.*, *47*, W04507, doi:10.1029/2009WR008969.

Cortis, A., and J. Birkholzer (2008), Continuous time random walk analysis of solute transport in fractured porous media, *Water Resour. Res.*, *44*, W06414, doi:10.1029/2007WR006596.

Dentz, M., and J. Carrera (2007), Mixing and spreading in stratified flow, *Phys. Fluids*, *19*, 017107, doi:10.1063/1.2427089.

Geiger, S., A. Cortis, and J. T. Birkholzer (2010), Upscaling solute transport in naturally fractured porous media with the continuous time random walk method, *Water Resour. Res.*, *46*, W12530, doi:10.1029/2010WR009133.

Grisak, G. E., and J. F. Pickens (1980), Solute transport through fractured media: 1. The effect of matrix diffusion, *Water Resour. Res.*, *16*(4), 719–730.

Hooker, J. N., S. E. Laubach, and R. Marrett (2013), Fracture-aperture size—Frequency, spatial distribution, and growth processes in strata-bounded and non-strata-bounded fractures, Cambrian Mesón Group, NW Argentina, *J. Struct. Geol.*, *54*, 54–71, doi:10.1016/j.jsg.2013.06.011.

Houseworth, J. E. (2006), An analytical model for solute transport in unsaturated flow through a single fracture and porous rock matrix, *Water Resour. Res.*, *42*, W01416, doi:10.1029/2004WR003770.

Liu, H.-H., G. S. Bodvarsson, and G. Zhang (2004), Scale dependency of the effective matrix diffusion coefficient, *Vadose Zone J.*, *3*, 312–315.

Maloszewski, P., and A. Zuber (1985), On the theory of tracer experiments in fissured rocks with a porous matrix, *J. Hydrol.*, *79*, 333–358.

Maloszewski, P., and A. Zuber (1990), Mathematical modeling of tracer behavior in short-term experiments in fissured rocks, *Water Resour. Res.*, *26*(7), 1517–1528.

Matthäi, S. K., H. M. Nick, C. Pain, and I. Neuweiler (2009), Simulation of solute transport through fractured rock: A higher-order accurate finite-element finite-volume method permitting large time steps, *Transp. Porous Media*, *83*, 289–318.

National Research Council (1996), *Rock Fractures and Fluid Flow: Contemporary Understanding and Applications*, Natl. Acad. of Sci., Washington, D. C.

Nelson, R. A. (1985), *Geologic Analysis of Naturally Fractured Reservoirs*, 2nd ed., Gulf Prof. Publ., Boston, Mass.

Neretnieks, I. (1980), Diffusion in the rock matrix: An important factor in radionuclide retardation, *J. Geophys. Res.*, *85*, 4379–4397.

Odling, N. E., and J. E. Roden (1997), Contaminant transport in fractured rocks with significant matrix permeability, using natural fracture geometries, *J. Contam. Hydrol.*, *27*, 263–283.

Pyrak-Nolte, L. J., and J. P. Morris (2000), Single fractures under normal stress: The relation between fracture specific stiffness and fluid flow, *Int. J. Rock Mech. Min. Sci.*, *37*, 245–262.

Robinson, N. I., J. M. Sharp Jr., and I. Kreisel (1998), Contaminant transport in sets of parallel finite fractures with fracture skins, *J. Contam. Hydrol.*, *31*, 83–109.

Roubinet, D., J.-R. de Dreuzy, and D. M. Tartakovsky (2012), Semi-analytical solutions for solute transport and exchange in fractured porous media, *Water Resour. Res.*, *48*, W01542, doi:10.1029/2011WR011168.

Rubin, H., A. M. Soliman, J. Birkhölzer, and G. Rouvé (1996), Transport of a tracer slug in a fractured permeable formation, *J. Hydrol.*, *176*, 153–180.

Rubin, H., D. Dveyrin, J. Birkhö1zer, and G. Rouvé (1997), Advection and dispersion of contaminant in a permeable medium embedding fractures in which advection velocity is comparatively slow, *J. Hydrol.*, *199*, 135–162.

Sharifi Haddad, A., H. Hassanzadeh, and J. Abedi (2012), Advective–diffusive mass transfer in fractured porous media with variable rock matrix block size, *J. Contam. Hydrol.*, *133*, 94–107, doi:10.1016/j.jconhyd.2012.02.008.

Sudicky, E. A., and E. O. Frind (1982), Contaminant transport in fractured porous media: Analytical solutions for a system of parallel fractures, *Water Resour. Res.*, *18*(6), 1634–1642.

Tang, D. H., E. O. Frind, and E. A. Sudicky (1981), Contaminant transport in fractured porous media: Analytical solution for a single fracture, *Water Resour. Res.*, *17*(3), 555–564.

Taylor, G. I. (1953), Dispersion of soluble matter in solvent flowing slowly through a tube, *Proc. R. Soc. London, Ser A*, *219*, 186–203.

Taylor, G. I. (1954), The dispersion of matter in turbulent flow through a pipe, *Proc. R. Soc. London, Ser A*, *223*, 446–468.

Thacker, W. C. (1976), A solvable model of "shear dispersion," *J. Phys. Oceanogr.*, *6*, 66–75.

Wooding, R. A. (1960), Instability of a viscous liquid of variable density in a vertical Hele Shaw cell, *J. Fluid Mech.*, *7*, 501–515, doi:10.1017/S0022112060000256.

Wu, Y.-S., and K. Pruess (2000), Numerical simulation of non-isothermal multiphase tracer transport in heterogeneous fractured porous media, *Adv. Water Resour.*, *23*, 699–723.

Zhan, H., Z. Wen, G. Huang, and D. Sun (2009), Analytical solution of two-dimensional solute transport in an aquifer–Aquitard system, *J. Contam. Hydrol.*, *107*, 162–174, doi:10.1016/j.jconhyd.2009.04.010.

Zhou, Q., H.-H. Liu, F. J. Molz, Y. Zhang, and G. S. Bodvarsson (2007), Field-scale effective matrix diffusion coefficient for fractured rock: Results from literature survey, *J. Contam. Hydrol.*, *93*, 161–187, doi:10.1016/j.jconhyd.2007.02.002.

DISCLAIMER

This document was prepared as an account of work sponsored by the United States Government. While this document is believed to contain correct information, neither the United States Government nor any agency thereof, nor The Regents of the University of California, nor any of their employees, makes any warranty, express or implied, or assumes any legal responsibility for the accuracy, completeness, or usefulness of any information, apparatus, product, or process disclosed, or represents that its use would not infringe privately owned rights. Reference herein to any specific commercial product, process, or service by its trade name, trademark, manufacturer, or otherwise, does not necessarily constitute or imply its endorsement, recommendation, or favoring by the United States Government or any agency thereof, or The Regents of the University of California. The views and opinions of authors expressed herein do not necessarily state or reflect those of the United States Government or any agency thereof or The Regents of the University of California.

Ernest Orlando Lawrence Berkeley National Laboratory is an equal opportunity employer.